A Novel Ocean Scatterometer for Simultaneous Measurements of Marine Winds and Surface Currents

Franco Fois(1), Peter Hoogeboom(1), François Le Chevalier(1), Ad Stoffelen(2), Alexis Mouche(3)

(1) Delft University of Technology, (2) KNMI, (3) IFREMER

TU Delft
Delft University of Technology

Royal Netherlands
Meteorological Institute
Ministry of Infrastructure and the Environment

Introduction

- The general circulation of the ocean is driven horizontally and vertically by two main mechanisms that are closely linked: wind driven circulation and density-driven thermohaline circulation.

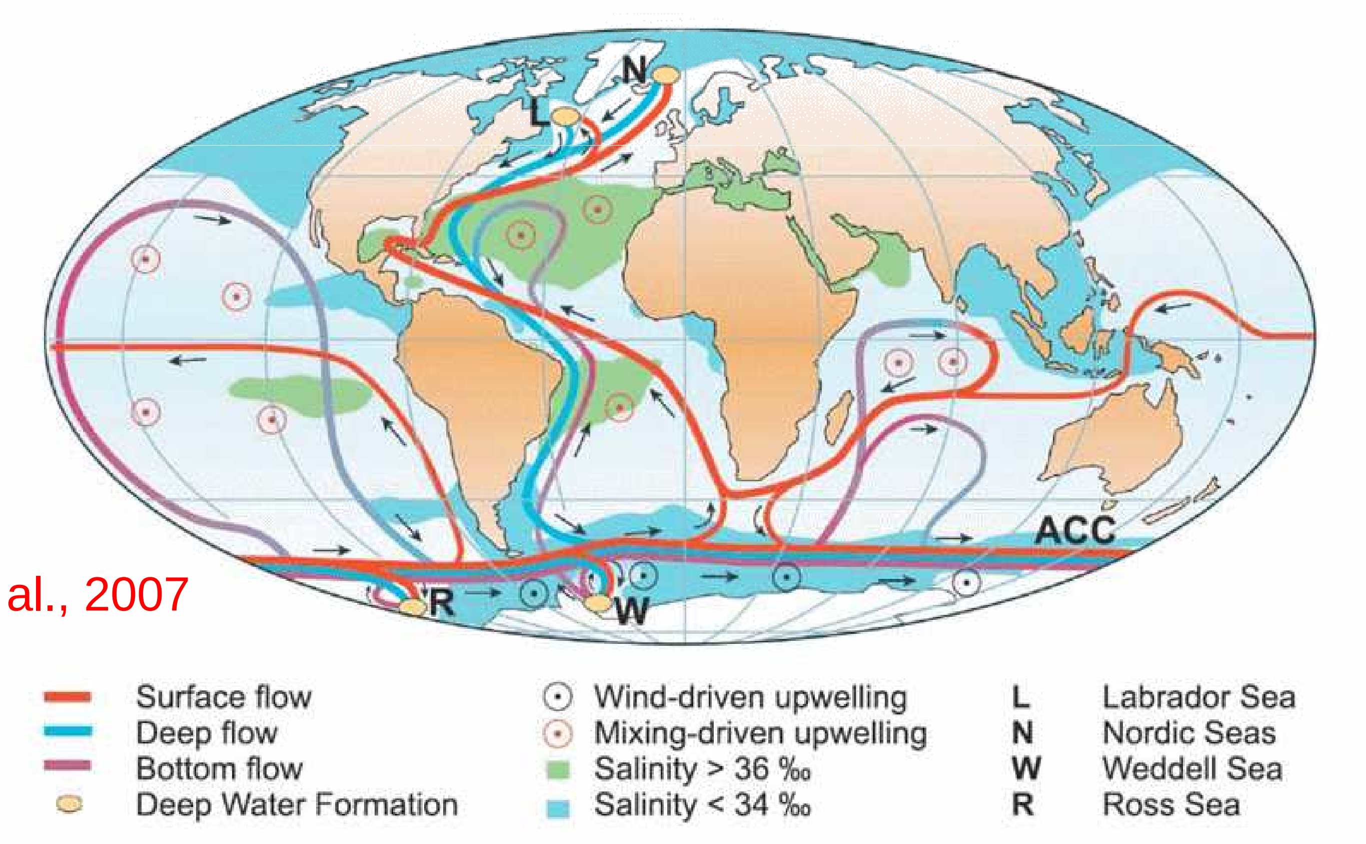

Kuhlbrodt et al., 2007

Introduction

- Wind driven ocean surface circulation is characterised by large ocean gyres. They include the western boundary currents (e.g. Gulf Stream, Kuroshio), eastern boundary currents (e.g. Canary current), equatorial currents, wind-driven and tidal flows.
- Thermohaline circulation is a much slower circulation process that is driven by deep-water convection in which surface cooling or the removal of freshwater (due to ice formation) leads to an increase in water density and the vertical descent of water.
- Deep convention occurs in the North Atlantic Ocean (forming North Atlantic Deep Water) and around Antarctica (forming Antarctic Bottom Water).

Ocean Surface Currents

- Ocean surface currents are the coherent horizontal and vertical movement of surface ocean water with a given velocity and an upper boundary in contact with the atmosphere that persist over a geographical region and time period.
- The average characteristic speed of horizontal currents is ~0.01-1.0 m/s (with large regional and local variations of >5 m/s) and is significantly larger than vertical current speeds that are ~ 0.001 m/s in a stratified ocean.
- Measurements of ocean surface currents are essential to a large number of scientific and societal issues and are essential to our understanding of ocean circulation at all time and space scales.

Scientific Justification

- Ocean surface currents and eddies, at scales shorter than 100 km, play a key role in the transport of heat, carbon and nutrients in the ocean.
- Gaining knowledge on currents and eddies would lead to improvements in the ability of computer models to predict future climate changes.
- Eddies in the North Atlantic have typical radii of 20-30 km and velocities of 2.5 km/day. Ideally, measurements to be made must then be at spatial intervals of 10-20 km on a daily basis.
- For coastal applications, the constraints in terms of spatial resolution and revisit time are even more stringent.

User Requirements

- User requirements for ocean surface current measurements have been derived in the frame of ESA Global Current UCM.
- The majority of users request higher resolution products closer to the coast (1-2 km), 1-10 km for inland seas and 10-25 km spatial resolution for global products. An accuracy better than 0.2 m/s is required.

Application	Coverage	Accuracy [cm s^{-1}]		Spatial Res [km]		Temporal Res. [hr]		Length of Record [years]
		Thr.	Obj.	Thr.	Obj.	Thr.	Obj.	
Weather Service	Global	20	10	25	12.5	24	6	10+
Ocean Service	Global	20	10	25	12.5	24	1	10
Search and Rescue	Regional	20	10	5	1	24	1	5
Scientific Research	Regional	20	10	25	1	24	6	10
Marine Renewable Energy	Local	20	10	5	0.1	24	1	10
Pollution	Local	20	10	10	0.1	24	1	5
Sailing	Global	20	10	10	--	24	--	--
Ship Routing	Global	10	5	20	1	24	1	5
Wave Forecasting	Global	20	10	25	2	24	0.5	1
Oil and Gas	Local-Reg.	20	10	5	1	24	1	1
Marine Offshore	Global	20	10	25	10	24	6	10
Fisheries Management	Local	20	10	25	1	24	6	10

Mission Background

Satellites provide a wide range of data that can, in principle, be used to generate surface ocean current maps at different time and spatial scales depending on the techniques used.

Technique	Description	Technique	Description
Satellite Altimetry	provides estimates of surface ocean currents in geostrophic balance at a course resolution. The geostrophic balance holds only for currents having spatial scales larger than a few tens of kilometers and time scales longer than several days.	Thermal and Visible Imagery	represents a viable way of estimating advective ocean surface currents from sequential infrared satellite imagery, by means of the Maximum Cross-Correlation (MCC) technique. However, the MCC method is often limited by thermal imagery with low surface gradients and undesirable viewing conditions (e.g. cloud cover). The technique fails over areas that do not show strong and coherent features over several days.
Satellite Synthetic Aperture Radars (SARs)	provide accurate measurements of the surface current in line-of-sight through measurements of the Doppler centroid. The geophysical interpretation of the absolute Doppler centroid is only possible if the attitude of the platform is very well known. Only 1 component of the velocity vector can be retrieved.	Sun glitter Mean Square Slope	uses a transfer function that relates the sun glitter brightness contrast to the mean square slope contrasts. The method has been successfully applied to MODIS and MERIS sun glitter imagery of natural oil seeps. The results document significant benefit from the synergetic use of sun glitter and radar imagery for quantitative investigations of surface signatures of ocean phenomena, including internal waves and mesoscale ocean currents.

Mission Background

Technique	Description	Technique	Description
SAR Along Track Interferometry (ATI)	provides measures of the Doppler shift of the backscattered signal by performing a difference in phase between two images of the same area of the ocean, collected with a time-lag sufficiently shorter than the decorrelation time of the ocean. Only the line-of-sight of the velocity vector can be measured. Typically, ATI requires the use of two satellites flying in formation and this makes the costs of the mission development and operations very high.	GOCE	A primary goal of the GOCE mission is the global determination of the ocean's geostrophic current systems. GOCE provides estimates of the shape of the marine geoid in radial direction with centimeters precision over spatial scales of 100-200 km.
Scatterometry	provides estimates of the surface wind speed over the ocean based on surface roughness measurements. Differences between the winds from Numerical Weather Prediction (NWP) model and from scatterometers are used to estimate time-varying ocean surface currents. The satellite scatterometer winds are, in fact, derived from ocean roughness, which depends on the relative motion difference between air and sea, whereas NWP model winds are provided with respect to a fixed Earth reference frame.	Microwave Imager	can be used to derive sea-ice motion by following the displacement of brightness temperature features in sequential images. The procedure for the calculation of ice motion is based on the MCC method. The sea-level pressure data produced by the European Centre for Medium-Range Weather Forecasts (ECMWF) is used for the calculation of the geostrophic wind. The effect of the geostrophic wind is subtracted from the ice motion to generate ocean surface current maps.

Current and future EO missions can bring new information to surface ocean current products but their products are not optimized to estimate ocean surface currents [Donlon, 2013].

Delft University of Technology

Mission Background

Royal Netherlands Meteorological Institute
Ministry of Infrastructure and the Environment

- Scatterometers with an antenna that provides multiple views, global ocean coverage and simultaneous wind vector estimation, appear, at first glance, to be ideal candidates for ocean surface current mapping using Doppler shift information.
- Nowadays, radar scatterometers are primarily designed to measure wind speed and direction from ocean radar backscatter, with spatial resolutions of tens of kilometers and swath widths wider than thousand kilometers.
- As these instruments were not specifically designed for Doppler measurements, new observation principles and data processing techniques must first be developed and validated.

Mission Requirements

Topic	Requirements	Topic	Requirements
Space Segment	Single spacecraft carrying a C-band Doppler Scatterometer	Spatial Resolution	Nominal product: 25 x 25 km^2 and spatial sampling of 12.5 km, High resolution product:< 12.5 x 25 km^2 and spatial sampling of 6.25 km.
Mission Duration	>5 years duration	Radiometric Resolution	VV-pol 4m/s cross-wind: kp≤ 3% for θi ≤25°, kp≤ (0.175 θi – 1.375)% for θi >25°. VV-pol 25m/s up-wind: kp≤ 3% for all θi VH-pol 15m/s cross-wind: kp≤ 15%, VH-pol 40 m/s up-wind: kp≤ 5%.
Orbit	Same orbit of MetOp	Radiometric Bias	≤0.4 dB (1-sigma)
Minimum Incidence	20°	Radiometric Stability	≤0.1 dB (1-sigma)
Coverage	87% global coverage in 24 h	Radar Ambiguities	≤-19 dB
Measurement Capability	Simultaneous acquisition of the Ocean Vector Wind (OVW) and Ocean Vector Motion (OVM)	Calibration targets	Active transponders, corner reflectors and homogeneous distributed targets.
Measurement Geometry	The swaths are oriented at 45° (Fore-left), 90° (Mid-left), 135° (Aft-left), 225° (Aft-right), 270° (Mid-right) and 315° (Fore-right) with respect to the satellite ground track.	Calibration process	The external calibration process shall not interfere with the nominal instrument operation and shall be sized in order to minimize the effect of ground clutter contamination.
Polarisations	Simultaneous acquisition of VV and VH polarisations.	Geolocation	≤ 2 km

Observation Principle

- The mission concept consists of a single satellite carrying a C-band Doppler scatterometer.
- The instrument is made of 6 slotted waveguide antennas, configured on three roof top shaped antenna assemblies.
- The 6 antennas are activated in sequence. The switching between the antennas is performed on a pulse to pulse basis.
- Each antenna transmits V-pol signals and receives simultaneously both V and H-pol echoes.

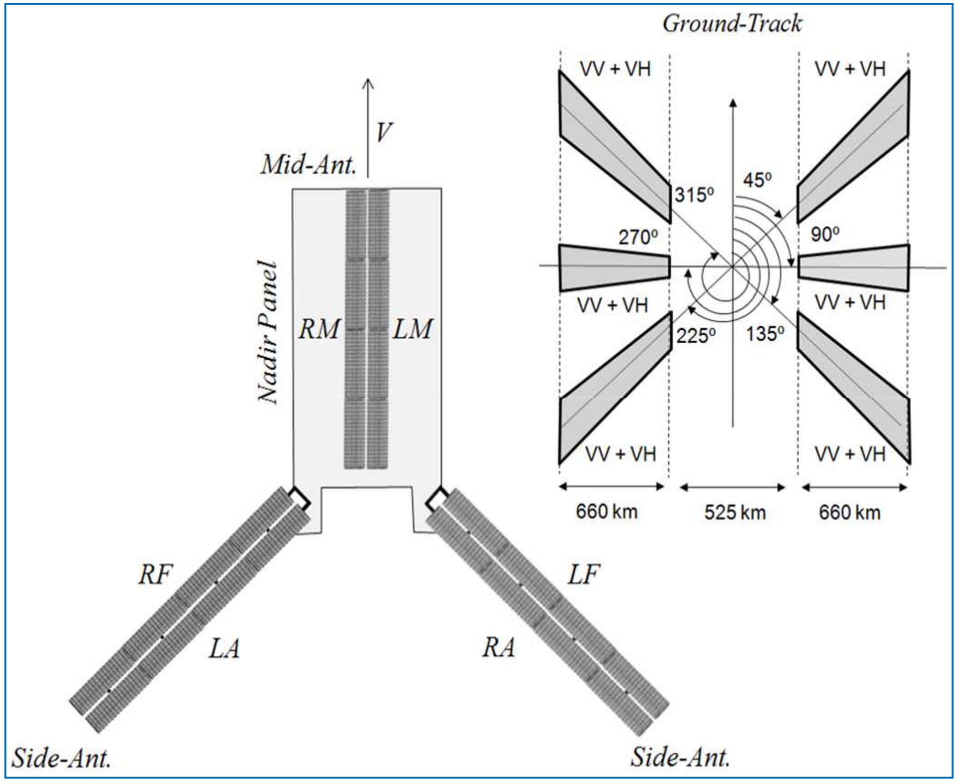

Geometry of observation of the C-band fan beam real aperture Doppler scatterometer

TU Delft
Delft University of Technology

Observation Principle

Royal Netherlands Meteorological Institute
Ministry of Infrastructure and the Environment

- DopSCAT transmits a dual chirp, that is a combination of an up-chirp, and a down-chirp.
- This waveform allows estimating not only the σ^o but also the Doppler shift of the ocean.
- The ambiguity functions of LFM pulses with opposite chirp rates are skewed in opposite direction, meaning that the introduced delay has an opposite sign.

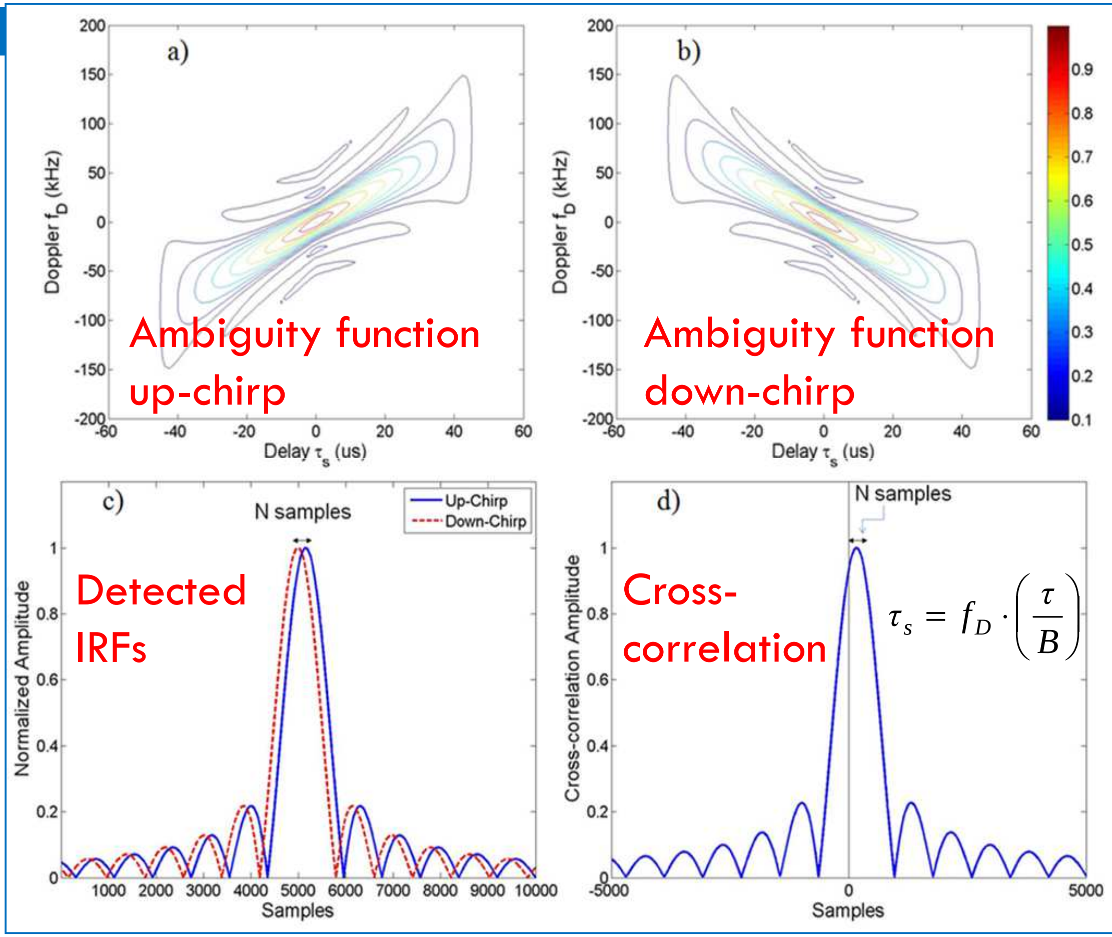

$$s(t) = s_u(t) + s_d(t) =$$
$$= \left\{ A \exp\left[j2\pi \left(f_c t + \frac{1}{2}\frac{B}{\tau} t^2 \right) \right] + A \exp\left[j2\pi \left(f_c t - \frac{1}{2}\frac{B}{\tau} t^2 \right) \right] \right\} \mathrm{rect}_{\tau}(t)$$

Instrument Concept

Royal Netherlands Meteorological Institute
Ministry of Infrastructure and the Environment

DOPSCAT Instrument block diagram

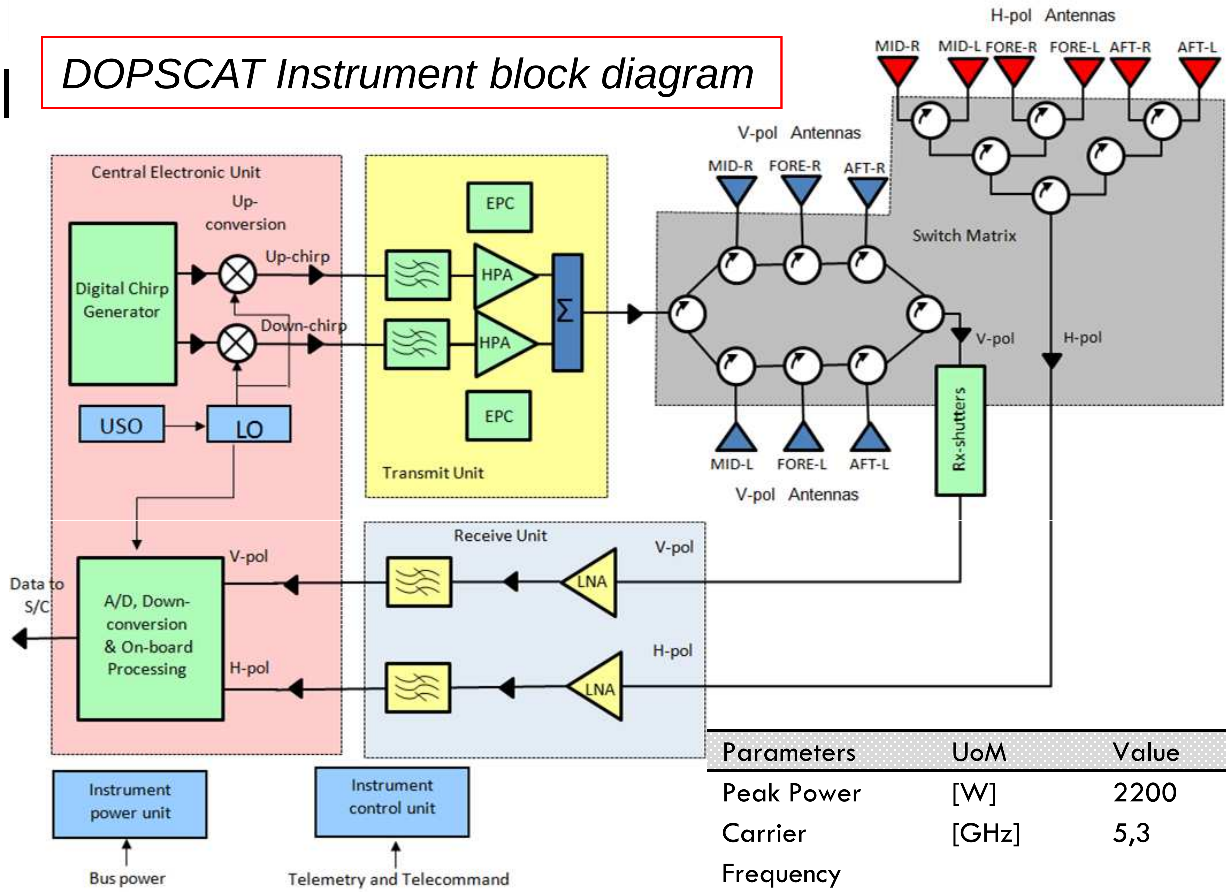

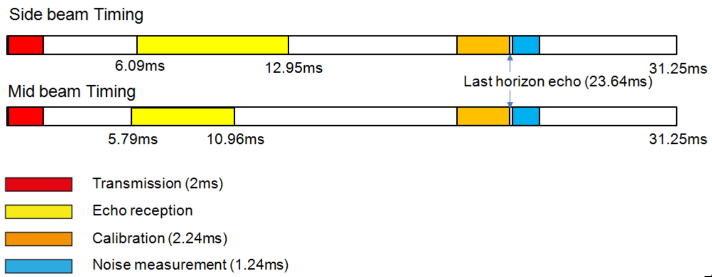

- Two receive chains are used to acquire simultaneously V & H-pol
- VH-pol is primary used for high-wind speed retrieval
- In this study, we also explore the possibility of using VH-pol together with VV-pol for surface current retrieval.

Parameters	UoM	Value	Parameters	UoM	Value
Peak Power	[W]	2200	MID-ANT Height	[m]	0,32
Carrier Frequency	[GHz]	5,3	SIDE-ANT Length	[m]	3,21
Pulse Duration	[ms]	2	SIDE-ANT Height	[m]	0.32
Tx signal	[#]	Double-chirp	Spatial Res.	[km×km]	25×25
ChirpRate [MID]	[kHz/ms]	417,5	Spatial Sampling	[km×km]	12,5×12,5
ChirpRate [SIDE]	[kHz/ms]	205	Number of Ant.	[#]	6
PRF	[Hz]	32	Pol. [MID-ANT]	[#]	VV and VH
Tx+Rx Losses	[dB]	3,4	Pol. [SIDE-ANT]	[#]	VV and VH
Noise Figure	[dB]	1,4	Swath Size	[km]	2×660
MID-ANT Length	[m]	2,87	Min. Inc. Angle	[°]	20

Avoiding Passive Intermodulation

- Two single-sideband transmit LFM pulses are generated, one with positive rate (up-chirp) and the other with negative rate (down-chirp).
- These pulses are up-converted to the carrier frequency by quadrature mixers and then amplified by two distinct High Power Amplifiers (HPAs).
- The use of two amplifiers instead of one avoids the generation of intermodulation products that might occur when the input to a non-linear device, such as the HPA, is composed of two frequencies.

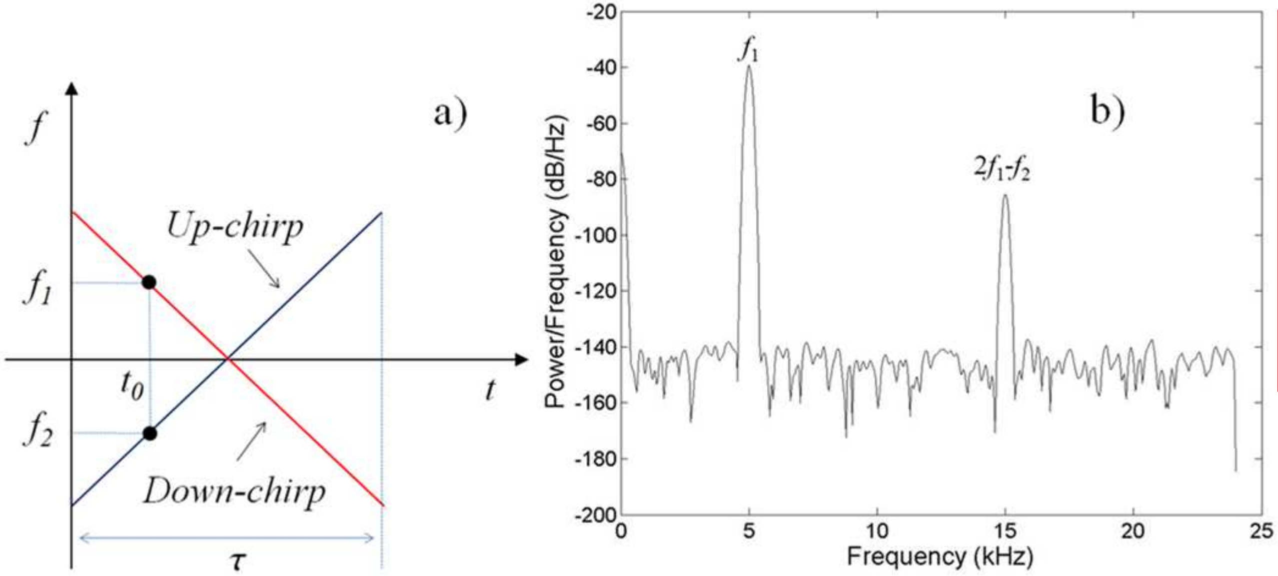

a) Transmit double-chirp signal; b) Power spectral density at the output of a HPA when the input waveform is the sum of two CW signals having frequencies f_1=-f_2= 5 kHz. The non linear transfer function of the HPA is $y= 0.5e\text{-}3x^3+1e\text{-}7x^2+0.1x+ 3e\text{-}3$.

Avoiding Passive Intermodulation

- As alternative, in order to avoid the use of two HPAs of 1.1 Kw each, the two chirps can be transmitted sequentially in time (one after the other).
- The advantage of this technique is the use of a single HPA, whereas the drawbacks are:
  - Both receive and calibration windows have to be increased to cope with the longer pulse;
  - Time-decorrelation effects may occur between the up-chirp and the down-chirp. However, at C-band, ocean echoes decorrelate in 20-40 ms depending on the wind conditions. Therefore a 2 ms separation between the two signals won't have any significant impact on the accuracy of the cross-correlation;
  - It will be more difficult to separate up-chirp echoes from down-chirp echoes with consequent increase of the IRF sidelobes (and so degradation of the ambiguity performance over the well scenario).

Instrument XTalk

- Because of the significant difference in backscattering, VH-pol measurements will be contaminated by VV-pol echoes unless stringent constraints on the instrument cross-talk are imposed.
- In fact, the predicted VH-NRCS can be more than 25 dB lower than VV-NRCS at 15 m/s wind speed and 20° incidence angle.

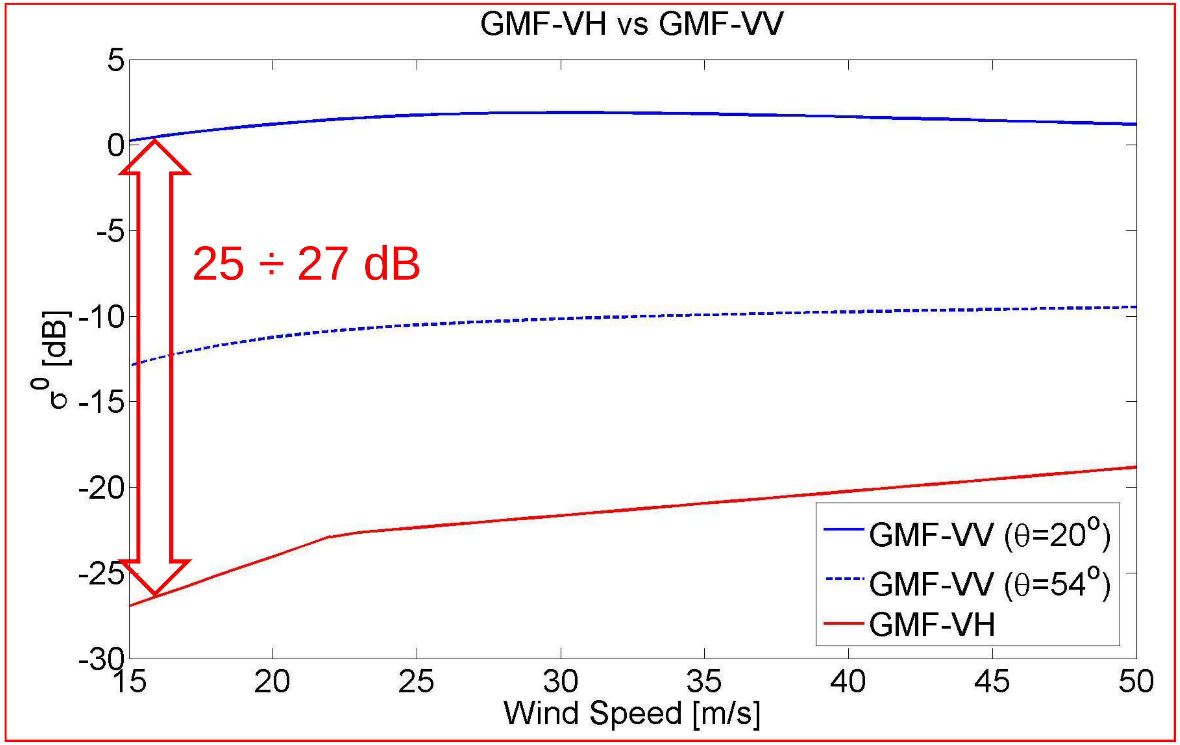

Instrument XTalk

- The ambiguity requirement asks for 1% ambiguity error at near swath (i.e. at 20°) with a wind speed within the well of 15 m/s.
- To simplify the problem and make it intuitive, let's focus only on what happens within the well and forget for a moment the ambiguous contributions arising from outside the well.

$$\frac{GTx_{VH}\cdot S_{HH}\cdot GRx_{HH}+GTx_{VV}\cdot S_{VV}\cdot GRx_{VH}}{GTx_{VV}\cdot S_{VH}\cdot GRx_{HH}}\le 0.01$$

$$S_{VV}\approx S_{HH} \qquad GTx_{VH}\approx GRx_{VH} \qquad GTx_{VV}\approx GRx_{HH}$$

$$\Downarrow$$

$$2\left(\frac{GRx_{VH}}{GRx_{HH}}\right)\left(\frac{S_{VV}}{S_{VH}}\right)\le 0.01$$

$$\Downarrow$$

$$\left[2\left(\frac{GRx_{VH}}{GRx_{HH}}\right)\left(\frac{S_{VV}}{S_{VH}}\right)\right]_{dB}\approx 3dB+Xtalk_{dB}+25dB\le -20dB$$

$$\Downarrow$$

$$\boxed{Xtalk_{dB}\le -48dB}$$

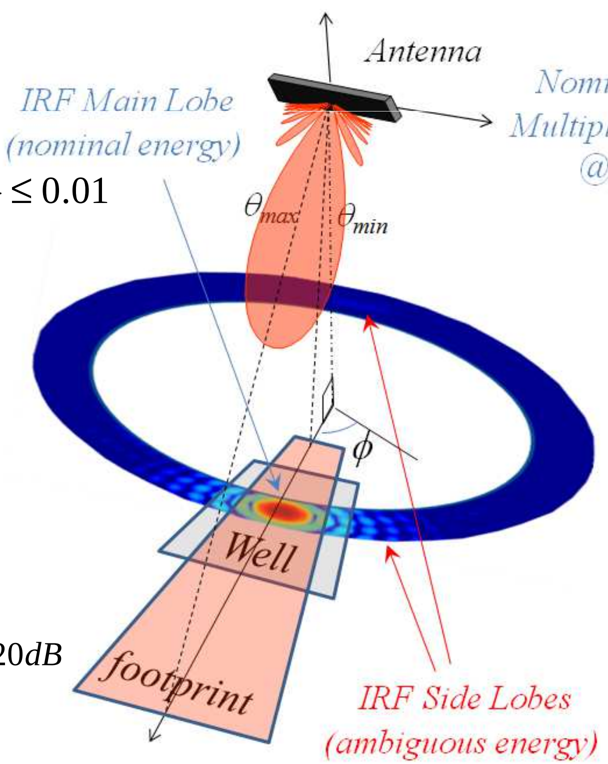

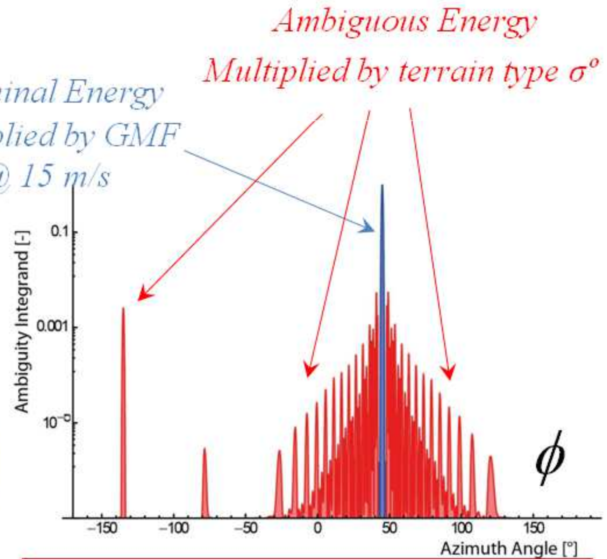

$$\boxed{\begin{aligned}M_{vh} &= Gtx_{vv}\cdot S_{vh}\cdot Grx_{hh} + \\ &Gtx_{vh}\cdot S_{hh}\cdot Grx_{hh} + Gtx_{vv}\cdot S_{vv}\cdot Grx_{vh} \\ &+ Gtx_{vh}\cdot S_{hv}\cdot Grx_{vh}\end{aligned}}$$

Level-1 Processing

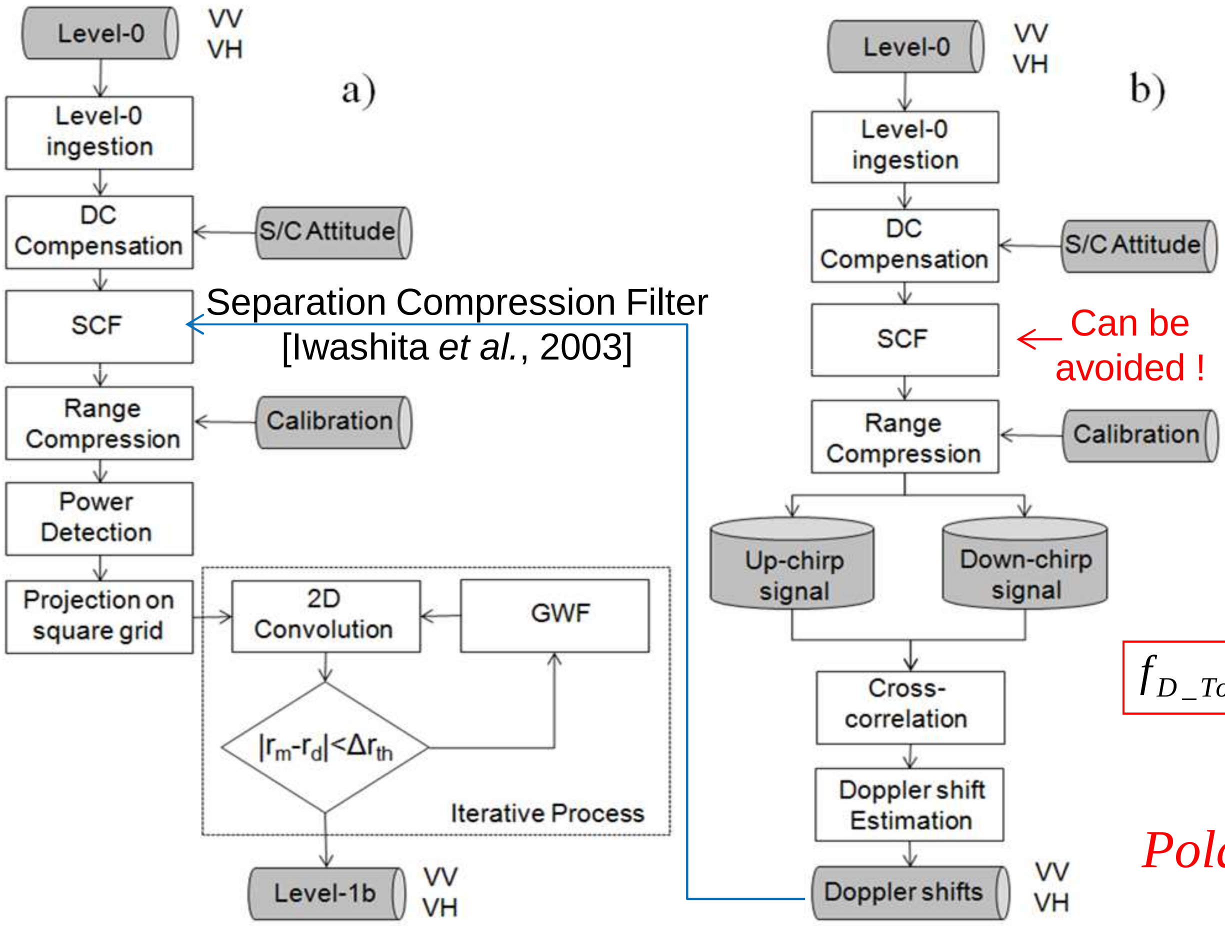

- The Doppler shift measured by a space-borne active microwave instrument over the ocean can be expressed as the sum of three main terms:

$$f_{D\_Total} = f_{D\_wind} + f_{D\_curr} + f_{D\_geo}$$

Polarization dependent

Polarization independent

Level-1 data processing flow for the generation of Normalized Radar Cross section images (left) and for the estimation ocean's Doppler shifts (right).

Accuracy of the Cross-correlation

- The Cramèr-Rao lower bound variance of the time delay estimate error about the true value is

$$\sigma^2_{t_{shift}} \geq \left\{ 2T \int_{f_1}^{f_2} (2\pi f)^2 \frac{|\gamma(f)|^2}{1-|\gamma(f)|^2} df \right\}^{-1}$$

[Quazi, 1982]

$$|\gamma(f)|^2 = \frac{S(f)^2}{[S(f)+N(f)]^2}$$

- The observation time T drives the spatial resolution r of the time-delay estimation

$$T = \frac{2r\sin\theta_{inc}}{c}$$

- The accuracy of the Doppler frequency estimation is:

$$\sigma_{f_D} = \sigma_{t_{shift}} \left(\frac{B_{pulse}}{\tau_{pulse}} \right)$$

- The accuracy improves with the number of along-track looks:

$$\sigma_{f_D}\Big|_{N_{obs}} = \frac{\sigma_{f_D}}{\sqrt{N_{obs}}}$$

$\gamma(f)$	Coherence function
T	Observation time
$S(f)$	Signal auto-spectrum
$N(f)$	Noise auto-spectrum
$B = f_2 - f_1$	Bandwidth
r	Desired resolution

Accuracy of the Cross-correlation

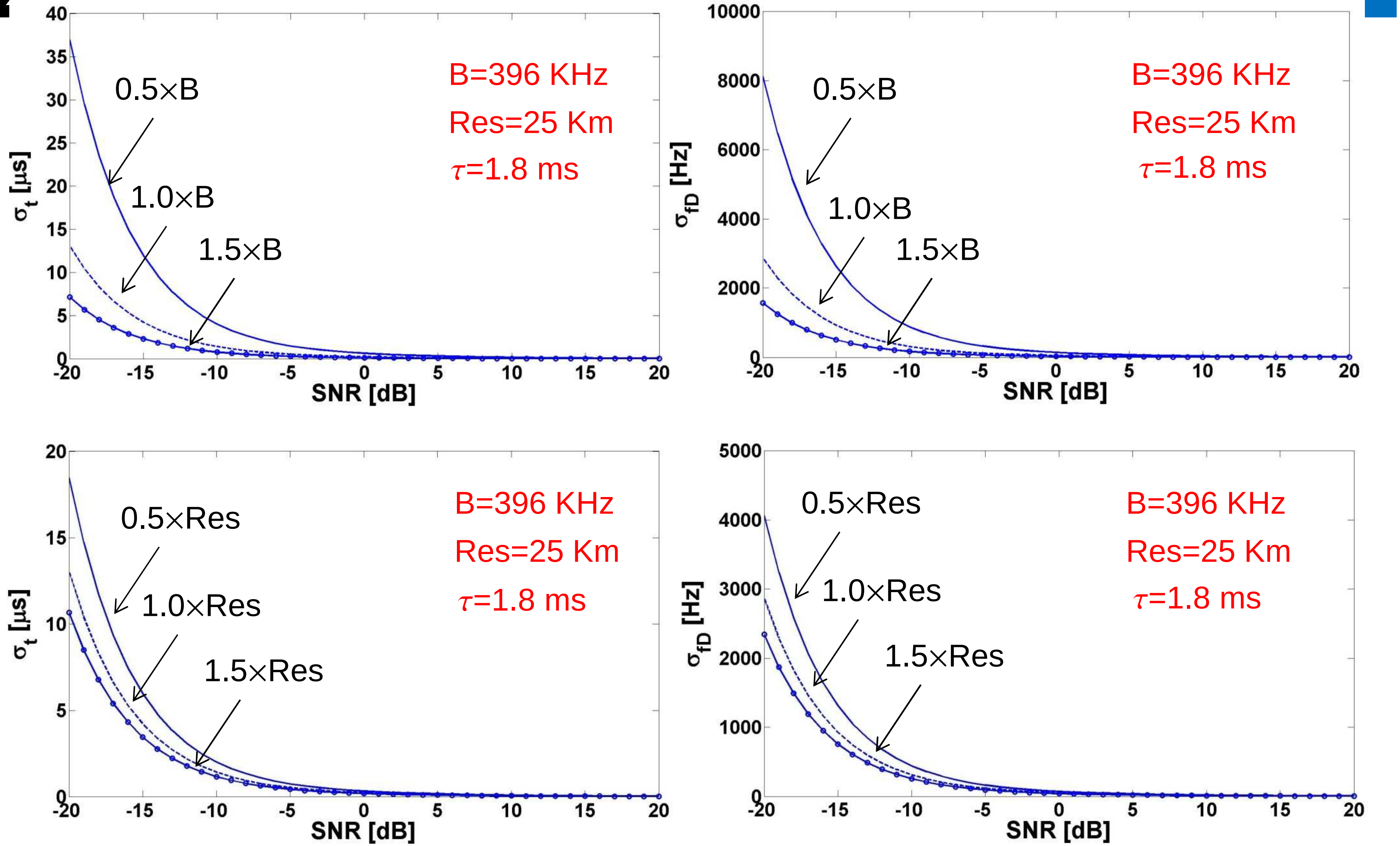

Accuracy of the Cross-correlation

- In the same Wind Vector Cell (WVC) we might be able to collect several (Nobs) Doppler measurements (one per Tx-pulse) depending on the Pulse Repetition Frequency of the scatterometer.
- As for the wind vector estimation, we will use these Nobs measurements to improve the accuracy of the Doppler estimate.

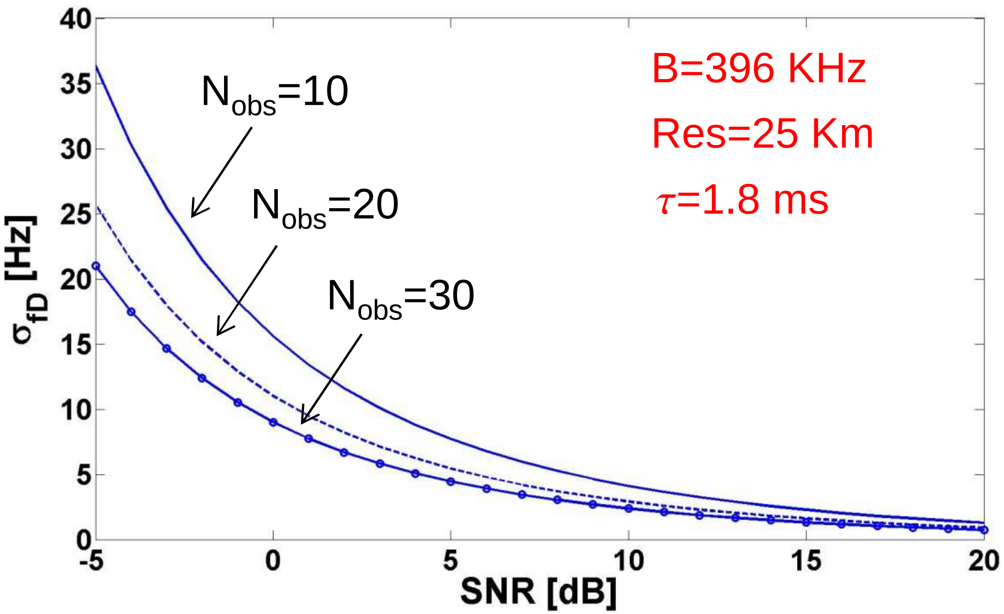

$$\sigma_{f_D}\Big|_{N_{obs}} = \frac{\sigma_{f_D}}{\sqrt{N_{obs}}}$$

$$N_{obs} = \frac{r_{Along-Track}}{V_{beam}\left(\dfrac{1}{PRF_{eff}}\right)}$$

V_{beam}	Beam velocity
PRF_{eff}	Effective PRF (per pol.)
$r_{Along-Track}$	Resolution

The Ocean Vector Motion

- Why the Doppler signature is so important? The Doppler signature is linked to the Ocean Vector Motion (OVM).

- Processes that generate OVM include wind stress, ocean waves, tidal forces, thermohaline dynamics, large-scale geostrophic flows, bathymetry, shoreline configuration and interaction between these processes (leading to complex ageostrophic flows).

- The OVM is a function of: wind drift, Stokes drift, Ekman current, tidal current, geostrophic current, ageostrophic current [Donlon, 2013].

The Ocean Vector Motion

- **Wind drift** is a real displacement of surface water associated with the direct frictional coupling between a thin layer (order cm) of the sea surface and the surface wind related to the roughness of the sea surface.

- **Stokes drift** is the mean temporal and spatial difference between the Eulerian and Lagrangian velocities associated with ocean surface gravity waves.

- **Ekman current** is the ocean surface flow generated by steady winds over the ocean, characterized by net flow of water at the surface at ~45° of the wind direction and a net integrated water transport at 90° of the wind direction. Ekman currents forms a spiral in the surface layer due to the balance between Coriolis and turbulent drag forces.

- **Tidal current** results from the gravitational forces exerted on the ocean by the moon and the sun.

The Ocean Vector Motion

- **Geostrophic current** is induced by the balance between the pressure gradient force and the Coriolis force resulting from the rotation of the Earth.

- **Ageostrophic current** results from the interaction between different flows connected with the deformation of the flow field such as surface divergence and/or convergence along ocean fronts, eddies and associated wind driven processes.

OVM Model

$$\mathbf{v}_{OVM} = \mathbf{v}_O^{wind} + \mathbf{v}_O^{curr} + \mathbf{v}_O^{\text{int}}$$

wind drift
Stokes drift

Ekman, Tidal,
Geostrophic currents

Interaction between different flows (i.e. ageostrophic current)

The wind-driven contribution

- The first term is polarization dependent and includes the motion due to the larger-scale metric waves together with Stokes drift, wind drift, short-wave motions and non linear hydrodynamic modulations of short waves by large waves.
- Below 30° incidence, the wind driven motion is dominated by large scale gravity waves which propagate faster. As the incidence angle increases, hydrodynamic modulations of short waves by large waves become the dominant contribution to the motion.

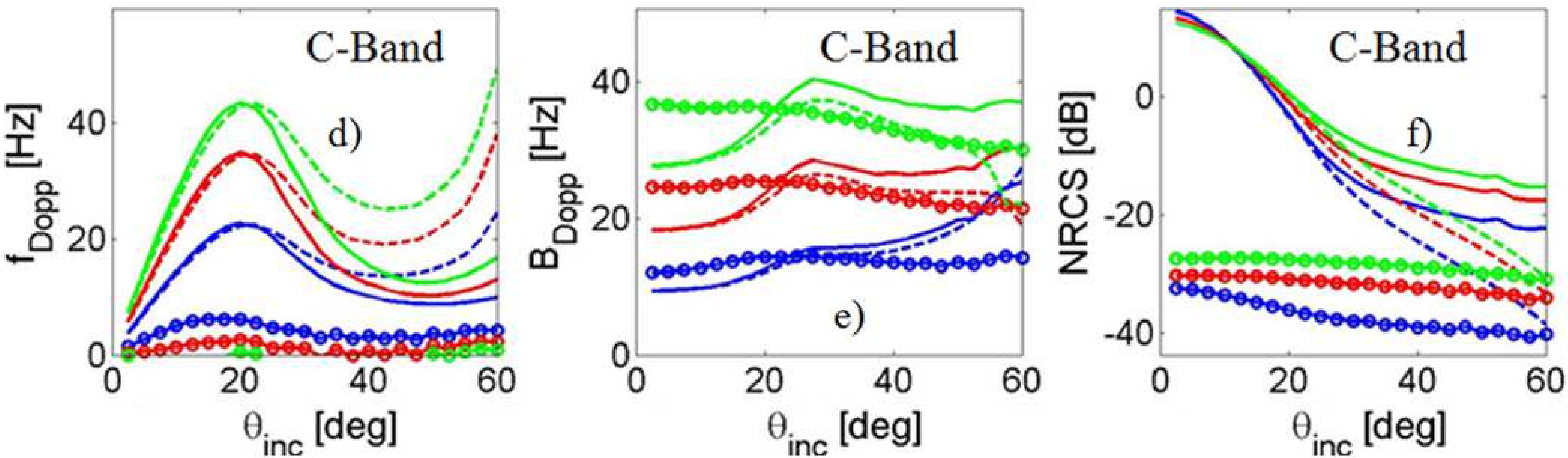

Fig. 1d)-f) Doppler shift, Doppler Bandwidth and NRCS computed by SSA2-CWM at C-band: green lines refer to 13 m/s wind speed (up-wind), whereas the red and blue lines refer to 9 and 5 m/s respectively. Dashed lines are used for HH, solid lines for VV and circles for VH.

Simplified relation between OVM and current

- In our study, the ageostrophic current term, that can be large in area of strongly varying surface current over short distances, is neglected.
- We assume that, at a resolution of a tens of kilometers (typical of ocean scatterometers) these rapidly varying surface currents are averaged out. Therefore, a simplified relationship between the sea surface current and the ocean motion vector is:

Simplified relation between OVM and sea surface current

$$\boxed{\mathbf{v}_O^{curr} \approx \mathbf{v}_{OVM} - \mathbf{v}_O^{wind}}$$

- Of course, this assumption will become questionable in coastal areas where surface current can be dominated by tidal currents modulated by complex bathymetry. However, for global ocean monitoring, this is an acceptable assumption.

The SSA2-CWM GMF

- One of the objective of the PhD was to derive a unified theory for the description of both microwave scattering and Doppler signature of the ocean, for the estimation of $\mathbf{v}_O^{wind}$
- The small slope approximation (SSA) [Voronovich, 1994] can be applied to any wavelength, provided that the tangent of grazing angles of incident/scattered radiation sufficiently exceeds the rms slope of roughness.
- The SSA is the result of a Taylor expansion with respect to the powers of surface slopes. It is common practice to call SSA1 and SSA2 the expansion performed at the first and second order respectively, the second being able to estimate the cross-polarized component of scattering in the plane of incidence.
- The SSA2 model uses the wave height spectrum to compute both scattering and Doppler signatures of the ocean.

The wave height spectrum

- The properties of the surface wave spectrum depend on environmental parameters such as the local wind vector.
- Estimating the wave height spectrum is extremely challenging because of the wavelengths involved (from mm to kilometers).
- The spectral shape results from the solution of the energy spectral density balance equation.

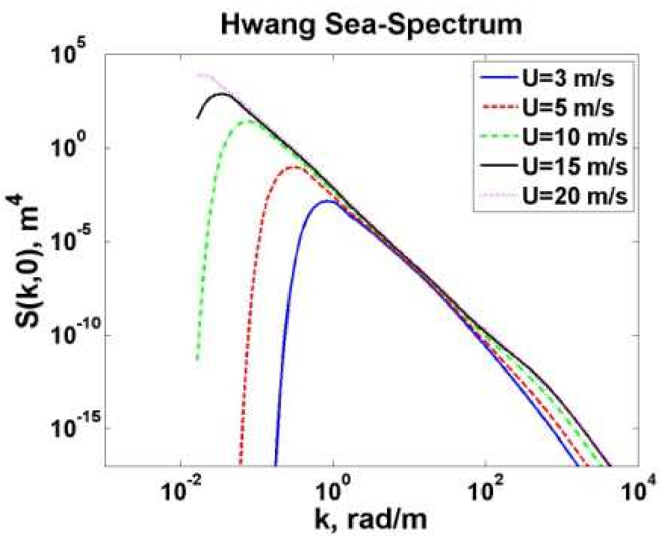

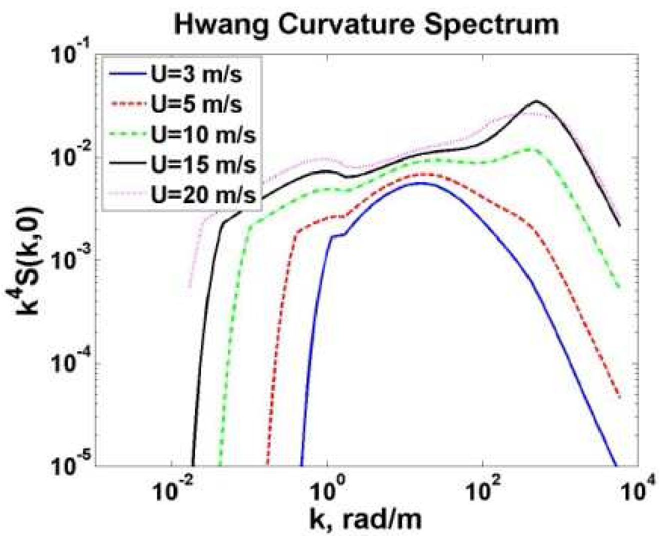

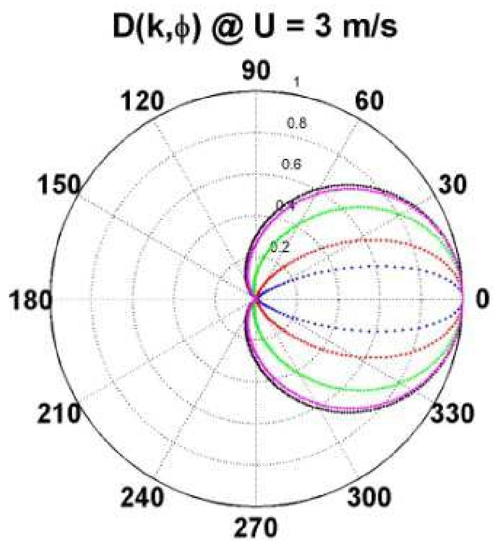

Delft University of Technology

The SSA2-CWM GMF

Royal Netherlands Meteorological Institute
Ministry of Infrastructure and the Environment

- The ocean sea surface is often represented by a Gaussian wave height distribution (linear sea-surface model).
- Non-linear hydrodynamic modulations of short waves by large waves change the statistics of the sea surface waves and cannot be ignored for a correct estimation of the sea surface Doppler signature.
- A numerically efficient weakly non-linear model, called “Choppy Wave Model” (CWM), is adopted in this work in combination with the SSA2.
- Being based on a description of the underlying physical phenomenon, this analytical model have the big potential of providing a more general and understandable relation between measured microwave ocean signatures (i.e. scattering and Doppler) and surface wind field than the empirical models.
- Considering the extended capabilities (e.g. larger incidence angle range, better spatial resolution, multi-polarisation observation capabilities) of DopSCAT as opposed to present and past scatterometers, the SSA2-CWM model function represents a very powerful tool that can support the design of the DopSCAT mission by extending the boundaries of CMOD and CDOP GMFs.

Validation of the SSA2-CWM GMF

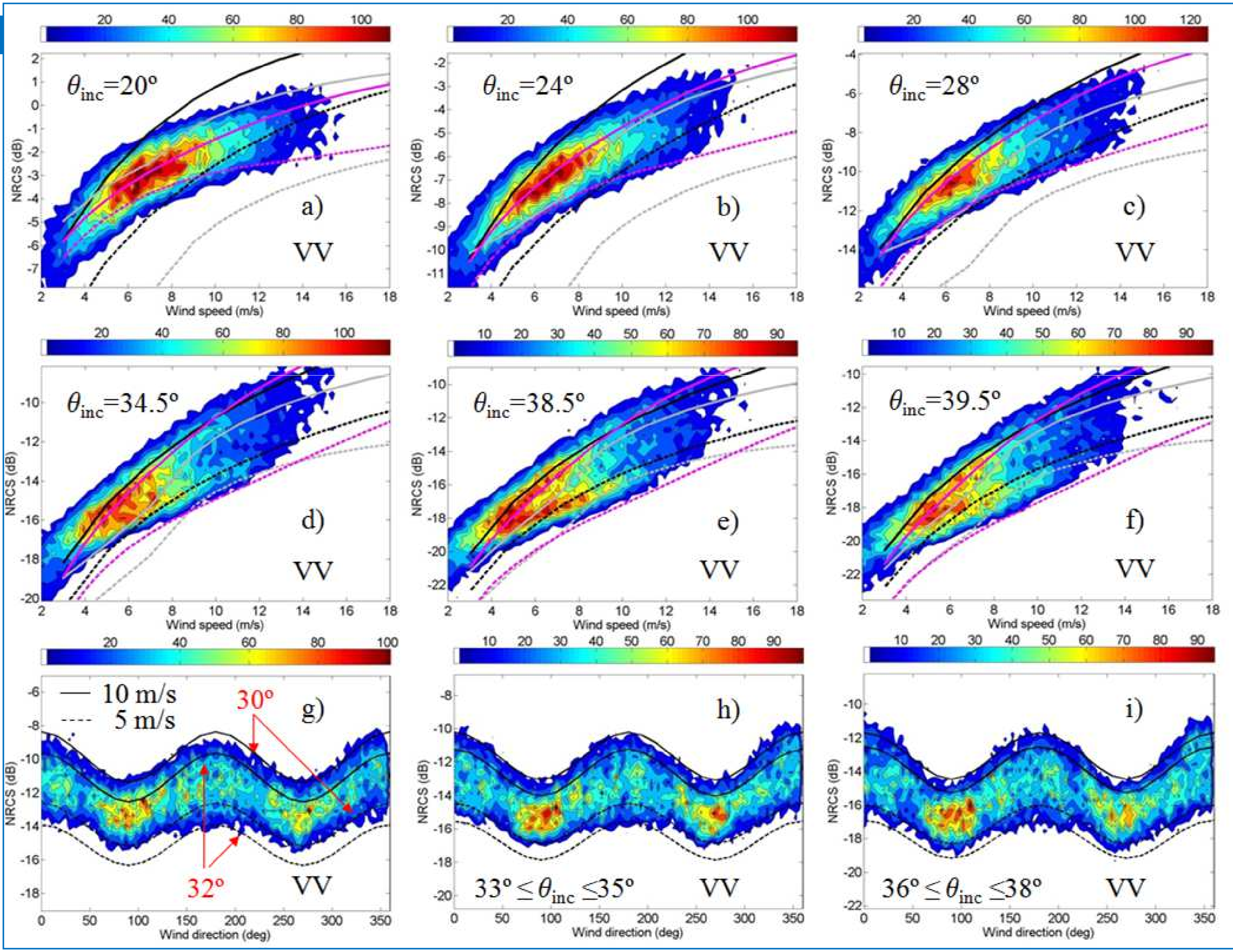

Validation of the SSA2-CWM GMF

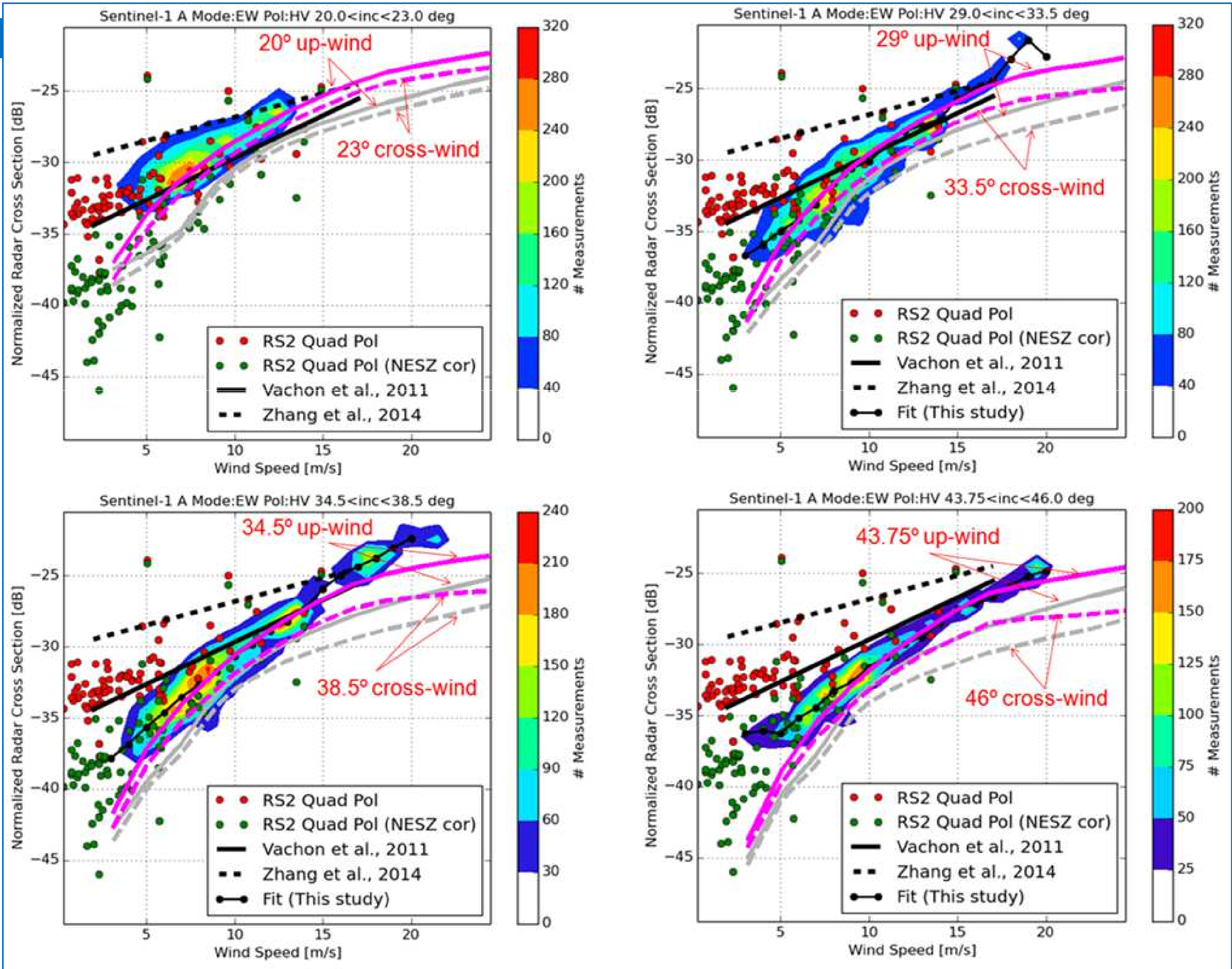

Validation of the SSA2-CWM GMF at high-winds

- Distribution of all retrieved SFMR wind speeds versus collocated VH measurement points from 9 RADARSAT-2 hurricane images. The red line shows the VH-GMF. Overlaid are the simulated cross-polar NRCS (in black) obtained in both up-wind and cross wind for four median incidence angles: 22.5°, 27.5°, 32.5° and 37.5°.

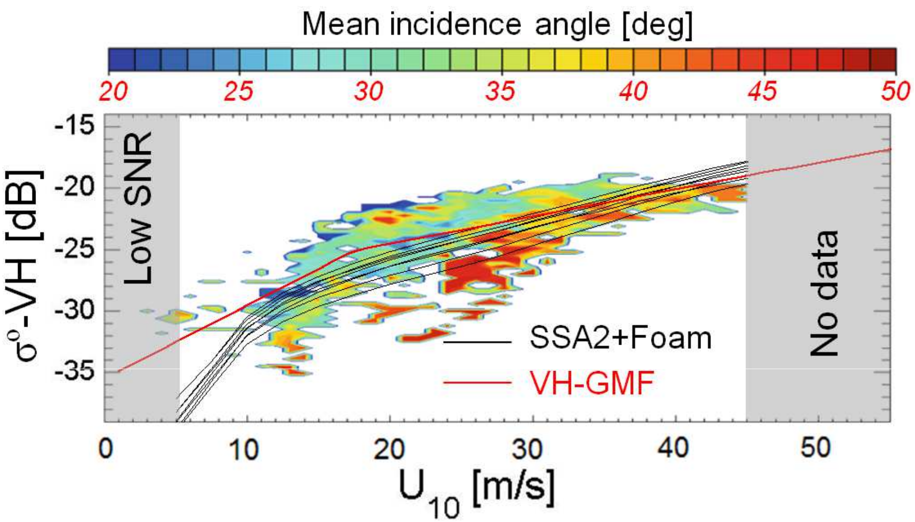

- Distribution of all forecasted ECMWF wind speeds versus collocated VH measurements from 19 hurricane RADARSAT-2 images

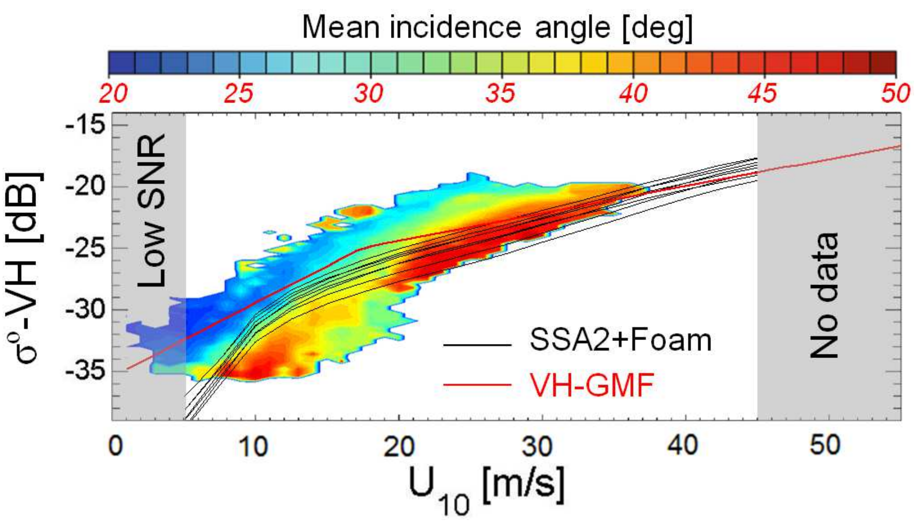

Validation of the SSA2-CWM GMF

- Joint distribution maps of observed ASAR Doppler anomaly (in C-band) and line-of-sight winds versus predictions given by SSA2-CWM (white curves) for up-wind (positive wind speed values) and down-wind cases (negative wind speed values). In dashed black the Doppler shifts provided by the CDOP empirical model and solid black the Doppler shifts as predicted by the High-frequency approximation of the scattering model, proposed by Mouche et al. in [2008].

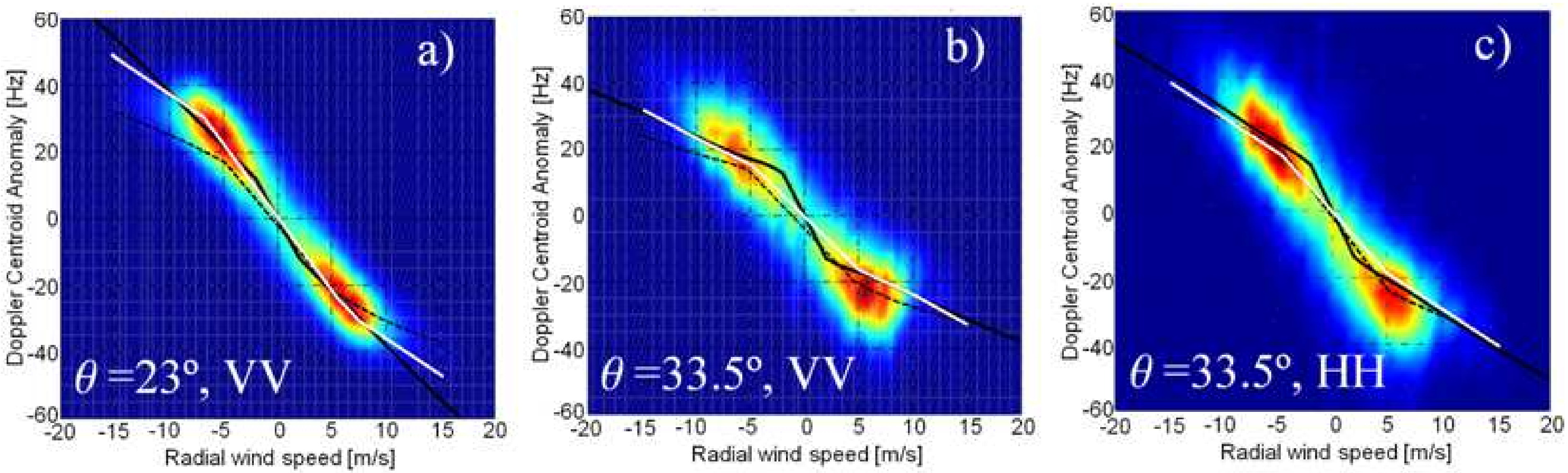

DopSCAT E2E Simulator

Delft University of Technology

Royal Netherlands Meteorological Institute
Ministry of Infrastructure and the Environment

- The DopSCAT E2E simulator is a tool to simulate and analyze the performance of the mission.

- We use the ASCAT data to generate wind velocity/direction maps and OSCAR data to generate ocean current scenarios.

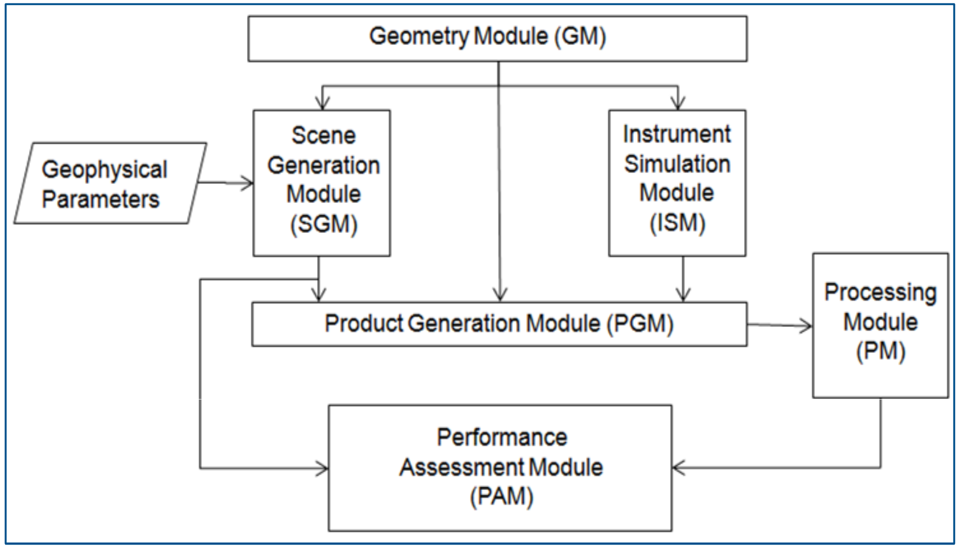

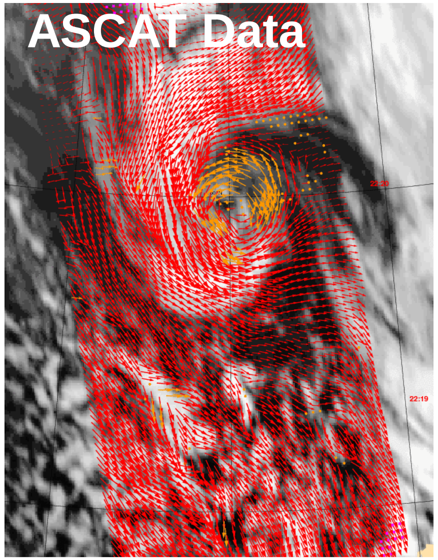

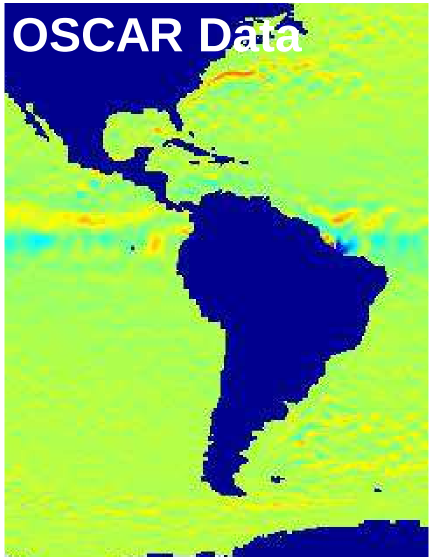

Geometry Module (GM)

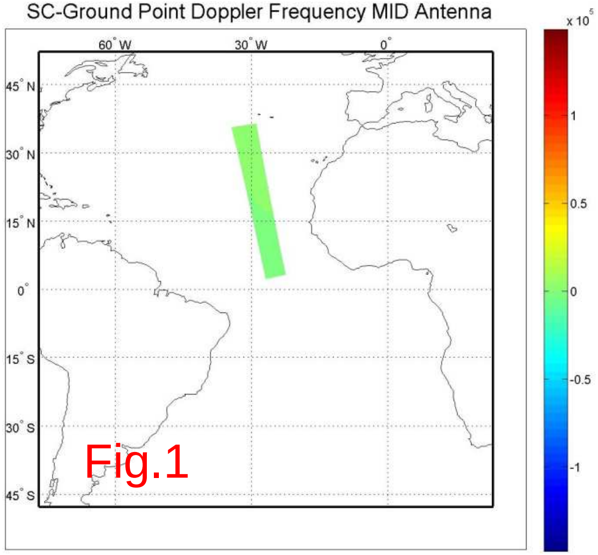

Fig.1

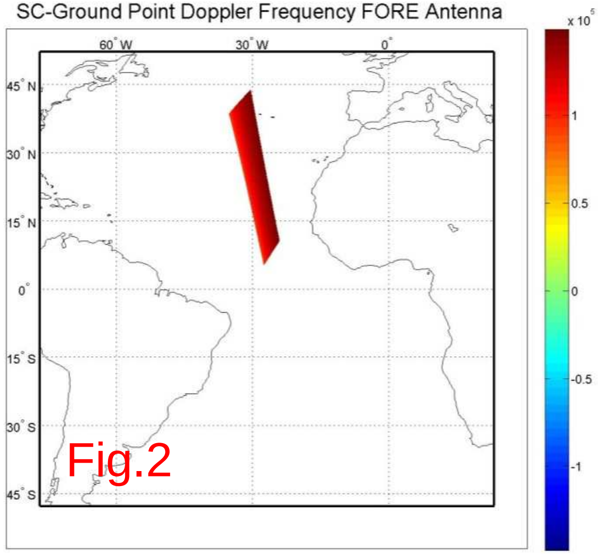

Fig.2

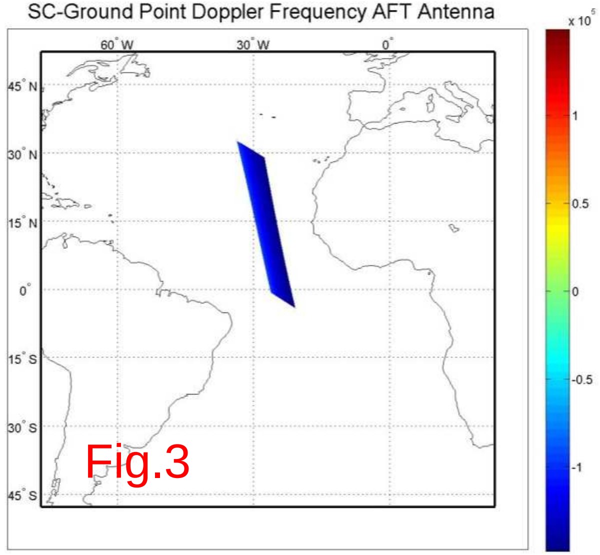

Fig.3

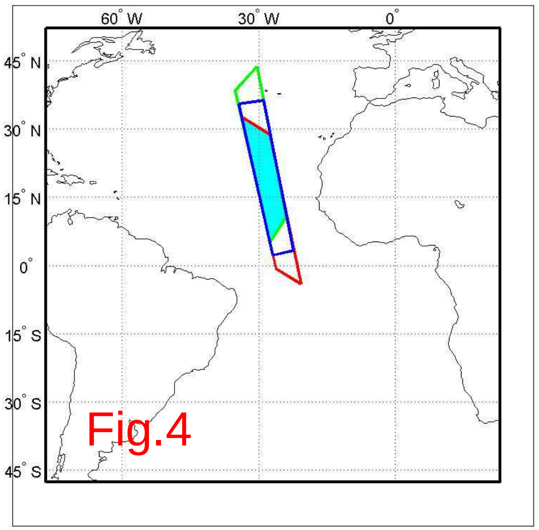

Fig.4

- The GM simulates the Metop-SG orbit.
- The geometric module computes for each WVC node all the associated geometrical parameters (e.g. slant range distances, geometrical Doppler frequencies, incidence angles, etc.)
- The GM identifies all the nodes observed by the three antennas (light blue area in Fig.4)

TU Delft
Delft University of Technology

Scene Generation Module (SGM)

Royal Netherlands Meteorological Institute
Ministry of Infrastructure and the Environment

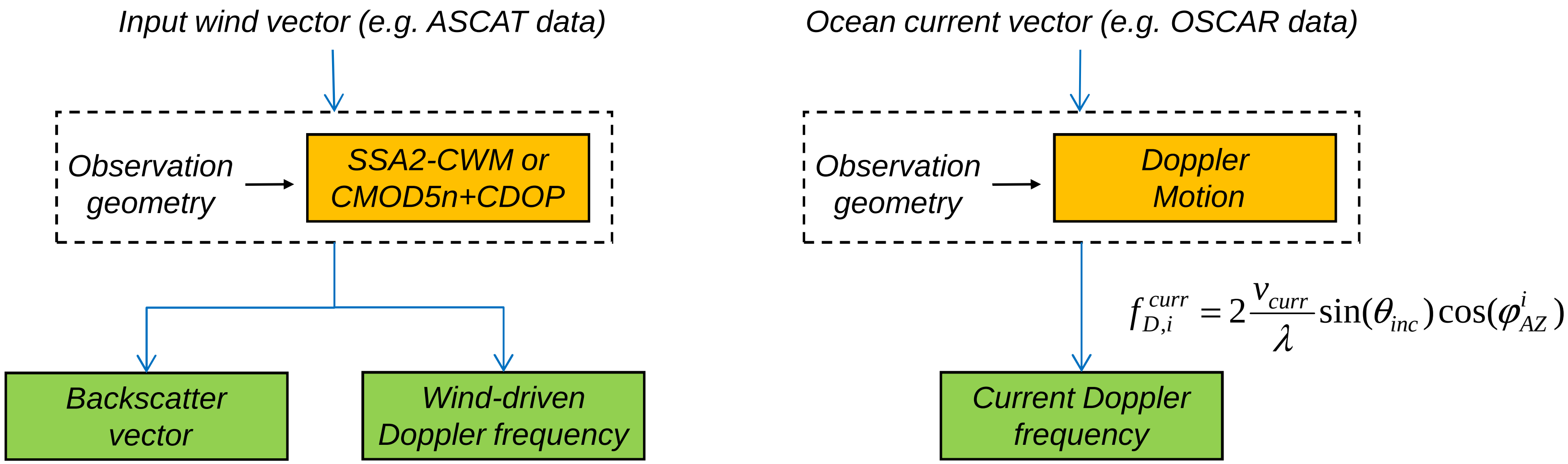

- The SGM generates backscattering maps for the MID, AFT and FORE antennas through the use of either SSA2-CWM or CMOD5n geophysical models.
- The SGM generates wind-driven Doppler frequency maps for the three antennas through the use of SSA2-CWM or CDOP empirical model function.
- The SGM computes also the Doppler frequency associated with ocean current vectors for each WVC.
- The novel SSA2-CWM model has been validated vs ASCAT, ASAR, RADARSAT-2 and Sentinel-1 data.

Delft University of Technology

SGM: Sigma0 maps

Royal Netherlands Meteorological Institute
Ministry of Infrastructure and the Environment

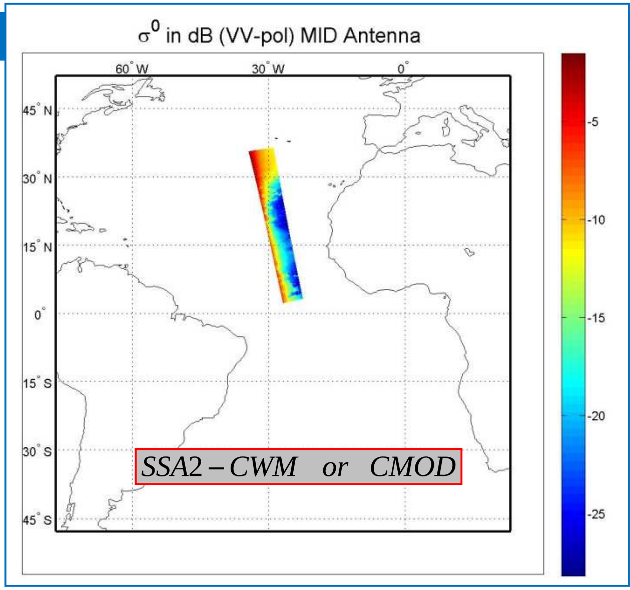

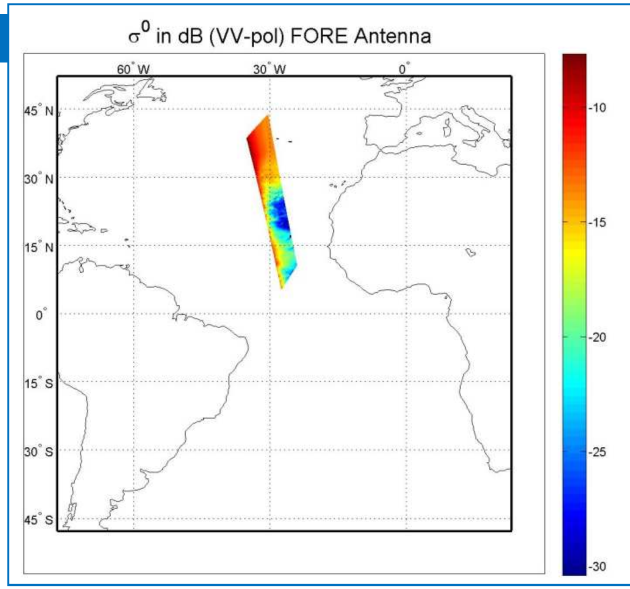

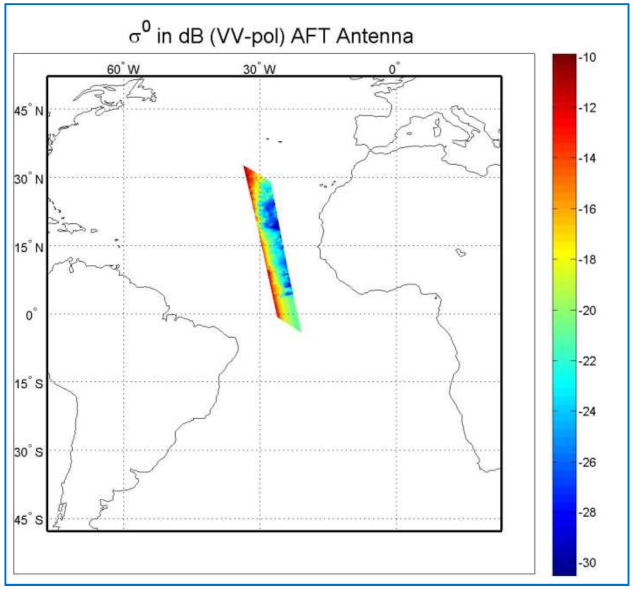

- The backscattering maps generated by the SGM do not yet include geophysical noise nor system noise. It will be a task of the Instrument Simulation Module (ISM) to add noise.

TU Delft
Delft University of Technology

SGM: Doppler shift maps

Royal Netherlands
Meteorological Institute
Ministry of Infrastructure and the Environment

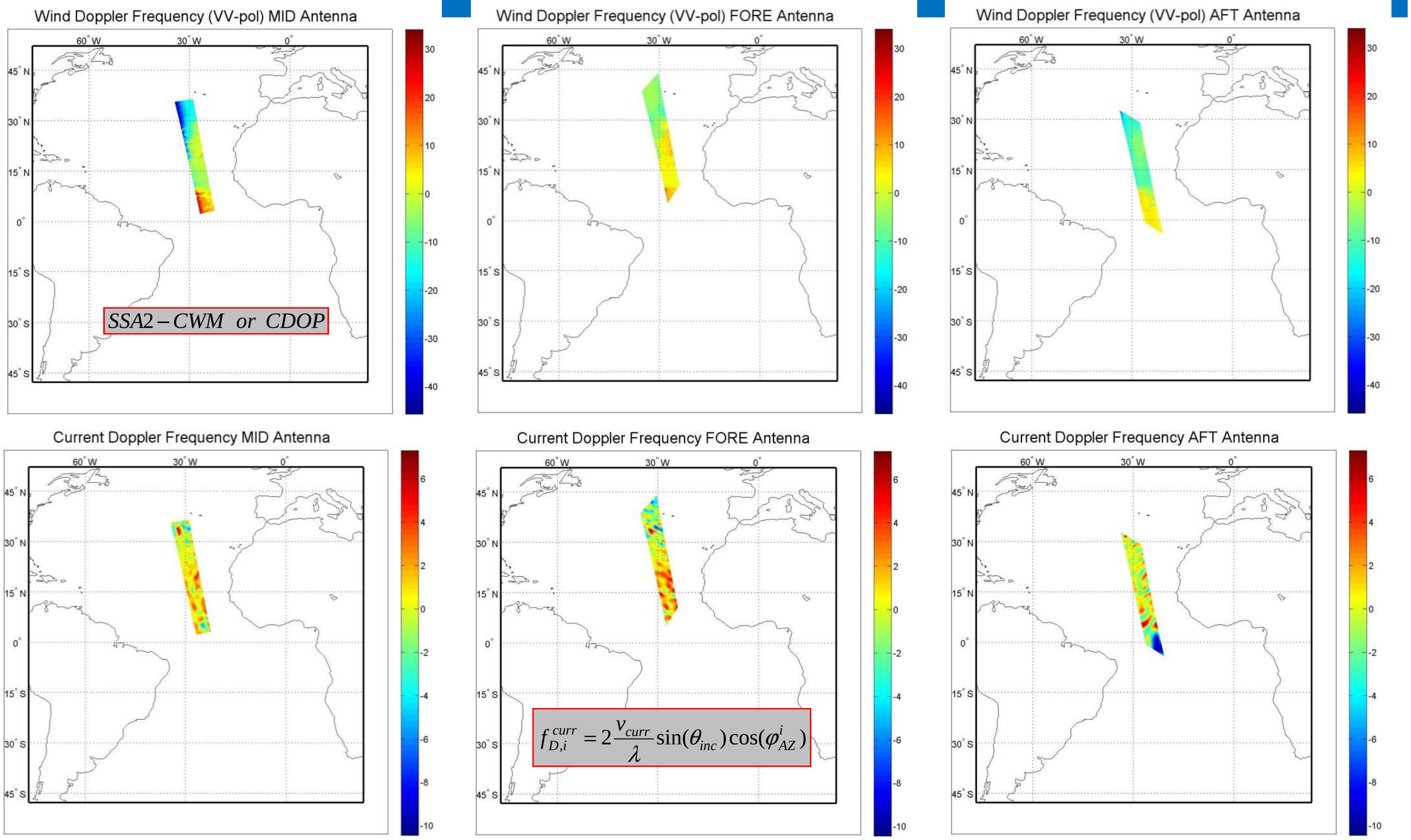

Instrument Simulation & Product Generation Modules

- The ISM computes both the SNR, and the radiometric resolution (Kp).

$$k_p = \sqrt{\frac{1}{N_A\ N_R}\left(1+\frac{1}{\left(\frac{S}{N}\right)^2}\right)+\frac{1}{N_N}\left(\frac{1}{\left(\frac{S}{N}\right)^2}\right)}$$

- The instrumental and geophysical noise contributions are assumed Gaussian and uncorrelated, thus:

$$\sigma^0 = \sigma^0_{GMF}\,(1+\sqrt{k_p^2+k_g^2}\cdot N[0;1])$$

$$f_D = (f_D^{GMF} + f_D^{Curr})\cdot (1+\sqrt{(\sigma^g_{f_D})^2+(\sigma^{X-corr}_{f_D})^2}\cdot N[0,1])$$

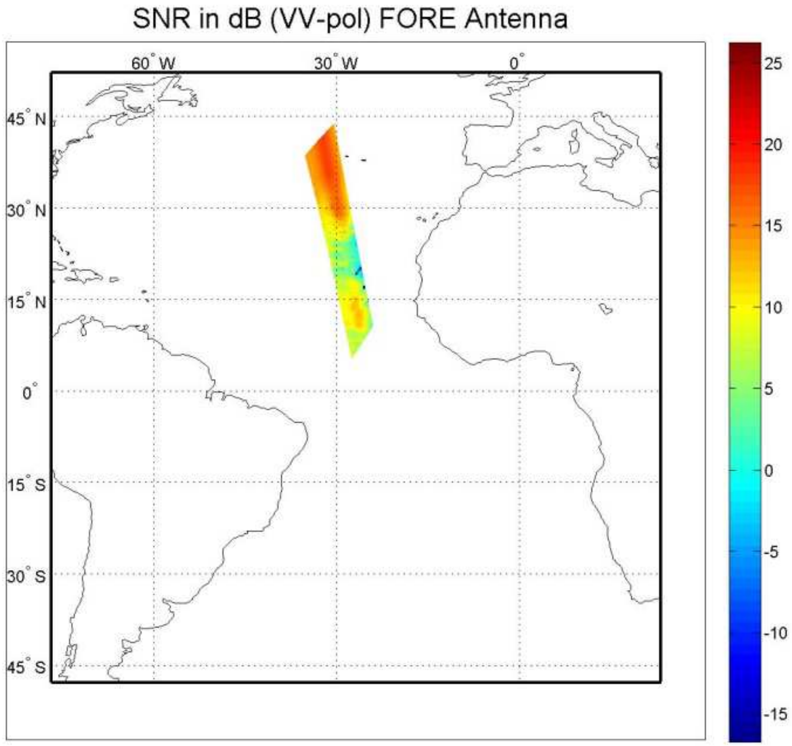

$$\frac{S}{N} = \frac{P_{Tx}\ G^2_{ant}\ \lambda^2\ \sigma^0\ \Theta^{azi}_{-1.5dB}}{(4\pi)^3\ d^3\ L_{TxRx}\ L^2_{atm}\left(\frac{\partial f_{total}}{\partial b}\right) k\ T\ n_f}$$

Instrument Simulation & Product Generation Modules

- Radiometric resolution (Kp) and accuracy of the cross-correlation function (σ^X_{fD}) over the MID and SIDE swaths for two extreme cases of winds

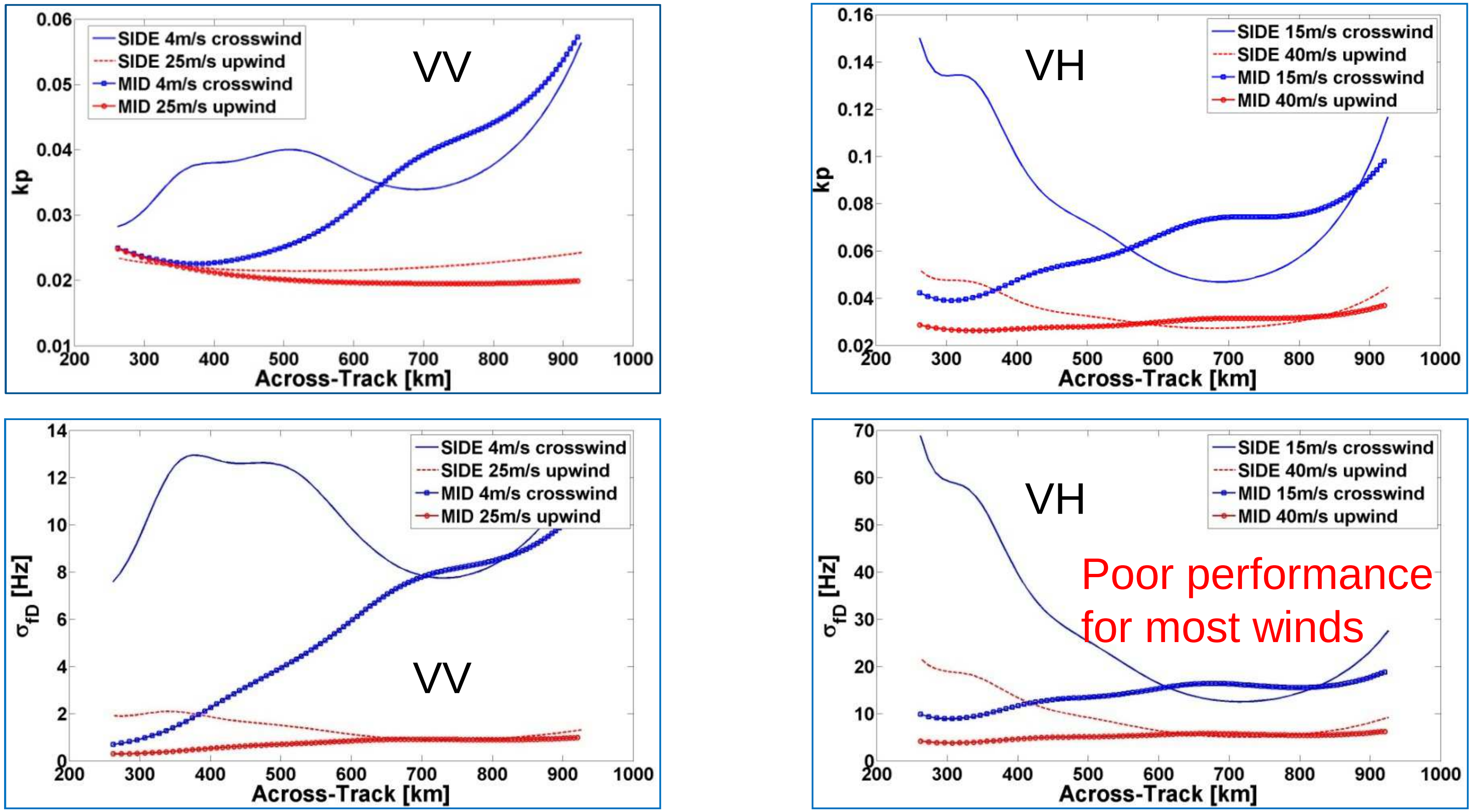

In VH the accuracy of the X-correlation function is too poor for surface current retrieval

TU Delft
Delft University of Technology

Processing & Performance Assessment Modules

Royal Netherlands Meteorological Institute
Ministry of Infrastructure and the Environment

- Extensive Monte-Carlo simulations show the capability of DopSCAT in estimating ocean currents with accuracy below 0.2 m/s, at a spatial resolution of 25 km (i.e. spatial sampling of 12.5 km) and a temporal resolution of 24 hrs.
- High-resolution products have accuracy worse than 1 m/s in ocean current estimates, which is only sufficient to meet the users' needs on a monthly time scale by performing temporal averages over stable currents.

$$MLE(\vec{v} \mid z) = \frac{1}{\langle MLE \rangle} \sum_{i=1\ldots N} \left| z_i - z_{GMF,i}(\vec{v}) \right|^2$$

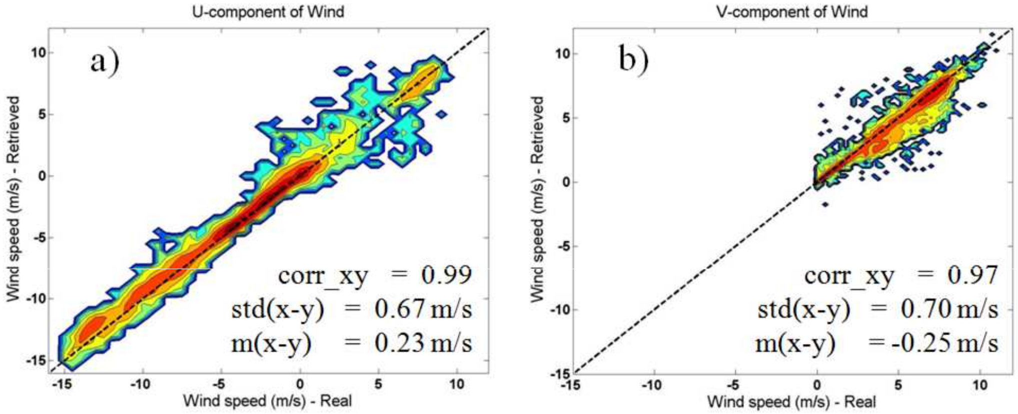

$$MLE(\vec{v}_{OVM} \mid f_D) = \sum_{i=1\ldots N} \left| f_{D,i} - \hat{f}_{D,i}(\vec{v}_{OVM}) \right|^2$$

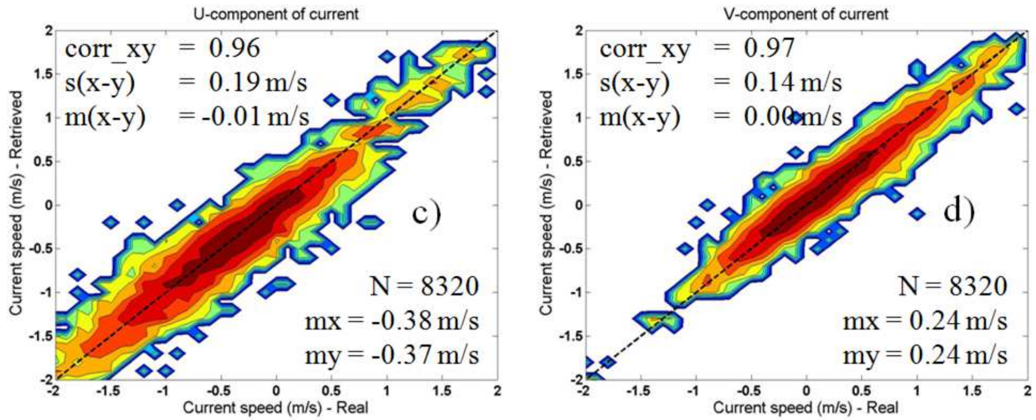

Oceanographic Validation of DopSCAT surface currents

Delft University of Technology

Royal Netherlands Meteorological Institute
Ministry of Infrastructure and the Environment

- In order to validate the method proposed to map the geophysical Doppler shifts into a sea surface current information, references for sea surface current measurements are needed. (e.g. Surface drifters, Argos buoys).
- The ocean surface currents over the globe are of many kinds. Various time and space scales as well as intensities of speed co-exist and it would be unrealistic to present DopSCAT as the ultimate solution for the study of all the types of currents.
- Ocean Doppler scatterometers could be used for daily global mapping to cover scales of a few tens of kms. This range scale constraints the selection of suitable regions for validation. In particular, narrow coastal currents, ocean fronts or tidal currents should be discarded.

Oceanographic Validation of DopSCAT surface currents

- A number of regions can be suitable for the validation of DopSCAT ocean current products. Among the Equatorial currents, we suggest the Equatorial Pacific current. This area is very well equipped with Tropical Atmosphere Ocean (TAO) buoys.

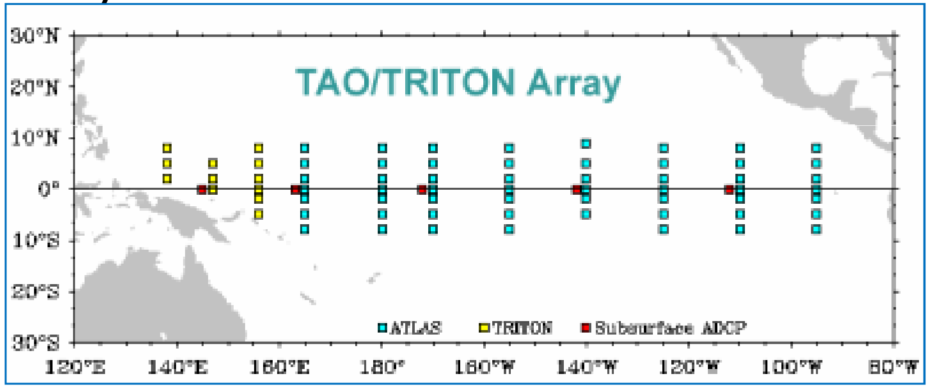

- Among the western boundary currents, the Agulhas and the Gulf stream are probably the most adequate sites. They are characterized by large, steady and intense flows.

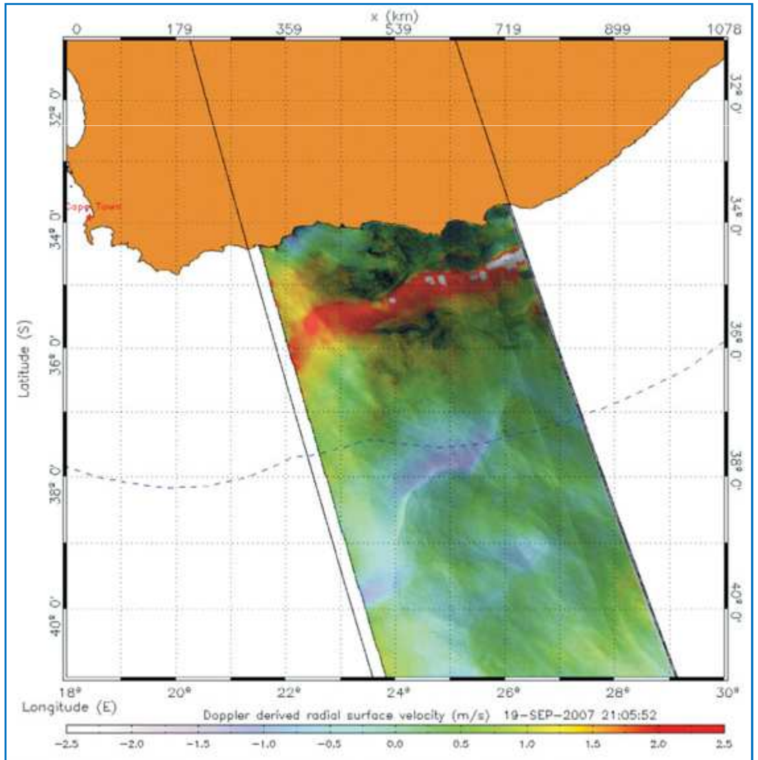

Fig. 1. Surface radial velocity in the Agulhas Current region. Credit: CLS radar division.

Oceanographic Validation of DopSCAT surface currents

TU Delft
Delft University of Technology

Royal Netherlands Meteorological Institute
Ministry of Infrastructure and the Environment

- A validation area such as the Gulf stream is also of interest because of the generation of ocean mesoscale eddies. The massive deployment of drifting buoys and co-located high-resolution high-frequency radar data by the NOAA's Integrated Ocean Observing System (IOOS) makes this area suitable for frequent ocean current calibration.

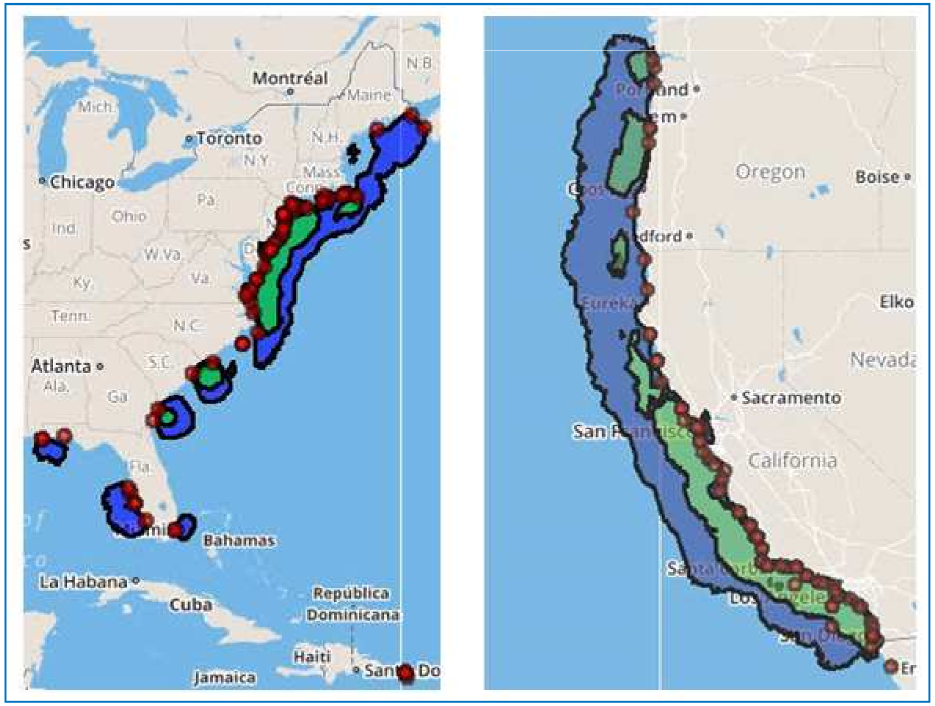

Oceanographic Validation of DopSCAT surface currents

- In order to verify whether the observed DopSCAT surface currents are of real nature, the use of co-located Sea Surface Temperature (SST) data from MetOp Advance Very High Resolution Radiometer (AVHRR) and Infrared Atmospheric Sounder Interferometer (IASI) would be of paramount importance, as SST gradients and fronts are typically linked to ocean currents.
- An instrument like IASI, if loaded on board the same satellite, would be able to fill the nadir gap left by DopSCAT ocean current product between -20° and +20° incidence.
- Another MetOp instrument that could be used in synergy with DopSCAT, for the purpose of its product validation, is the MicroWave Imager (MWI). The MicroWave Imager can be used to derive sea-ice motion by following the displacement of brightness temperature features in sequential images.

Conclusions

- The use of double chirps instead of classical up or down chirps enables Doppler shift to be estimated.
- No critical elements have been identified for the DopSCAT development. The DopSCAT subsystems are, in fact, entirely based on heritage from past and current C-band radar missions (e.g. MetOp's ASCAT, MetOp-SG's SCA, Sentinel-1, RADARSAT-2).
- The proposed mission design allows very good radiometric resolution in VV polarization. This enables precise estimation of the wind vector, that is a necessary condition for an accurate estimation of the ocean motion. VH-pol allows retrieving very high winds.
- DopSCAT provides simultaneous and accurate measurements of OWV OMV at a spatial resolution of 25 km (i.e. 12.5 km spatial sampling) on a daily basis with good coverage. These maps will allow gaining insights on the upper ocean dynamics at mesoscale.

Appendix: SCF & IRF performance

Delft University of Technology

Royal Netherlands Meteorological Institute
Ministry of Infrastructure and the Environment

- The Separation Compression Filter (SCF) is used to separate the dual chirp echo signal into an up-chirp component and a down-chirp component, thus avoiding undesired interferences from down-chirps to up-chirps and vice versa.
- Performance of the Separation Compression Filter (SCF) depends on the accuracy of the Doppler shift estimates.

Transmit-Signal

$$\boxed{s(t) = s_u(t) + s_d(t) \rightarrow S(f) = S_u(f) + S_d(f)}$$

$$\boxed{G_u(f) = \frac{S_d(f)}{S_u(f)} = \frac{R_d(f)}{R_u(f)}}$$

Receive-Signal

$$\boxed{r(t) = r_u(t) + r_d(t) = \sum_{i=1}^{N} r_u^i(t) + \sum_{i=1}^{N} r_d^i(t) \rightarrow R(f) = R_u(f) + R_d(f)}$$

SCF

$$\boxed{R_u(f) = \frac{R(f)}{I + G_u(f)}}$$

Appendix: SCF & IRF performance

- If we directly apply the SCF without any compensation of the Doppler shift, the quality of the Impulse Response Function (IRF) will be degraded (e.g. the sidelobes of the IRF will increase, the peak of the IRF will decrease).
- In order to avoid such undesired effects, the SCF has to be performed after the following sequential steps:
  1) geometrical DC compensation (by a priori geometrical and pointing knowledge);
  2) geophysical Doppler shift estimation (by cross-correlation of up and down chirps echoes);
  3) geophysical Doppler shift compensation (i.e. the estimated geophysical Doppler shift is used in building up the separation compression filter).

Appendix: SCF & IRF performance

- DopSCAT IRFs obtained with SCF (blue curves) and without SCF (red curves) for different Doppler shift errors (0, 10, 30, Hz).

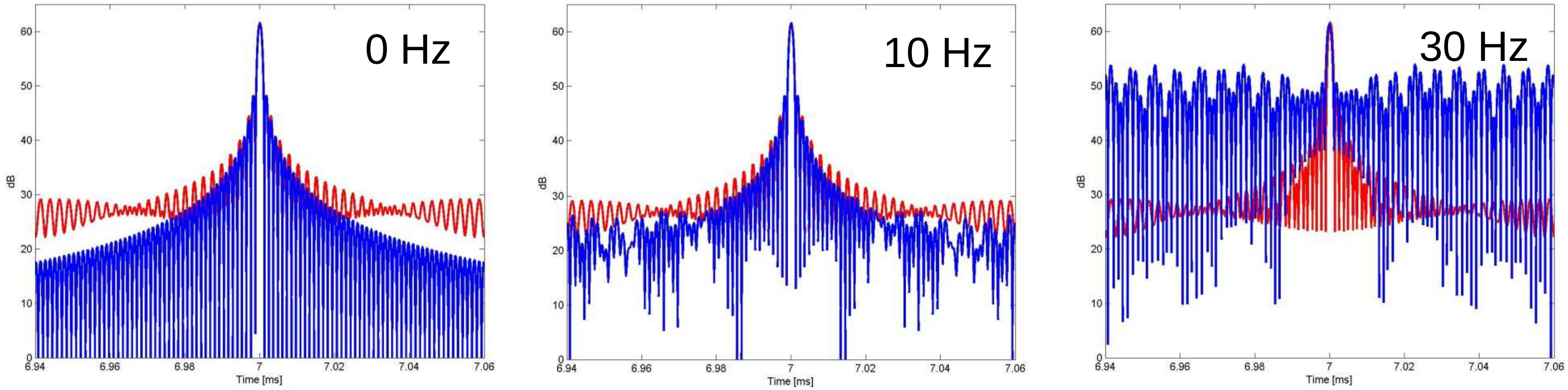

- For the proposed system concept, σ_{fD} is expected to be lower than 10 Hz in VV polarization and for most winds (between 4 m/s cross-wind and 25 m/s up-wind).
- An accuracy of 10 Hz has only a marginal impact on the IRF performance.

Appendix: Pointing errors

- The Doppler shift measurements as well as the NRCS measurements can be affected by pointing errors caused by:
  - errors in satellite orbit and attitude parameters;
  - thermoelastic distortions of the antenna subsystem;
  - electronic mispointing of the antenna subsystem.
- The error in Doppler measurement can be expressed in the following form:

$$\boxed{f_{Derr} = f_D - f_{Dp} = f_{Dpe} + f_{D\sigma^0} + f_{D\Delta}}$$

- where the 1st term is an error in the prediction of the Doppler shift caused by a mispointing of the antenna beam, the 2nd term is a Doppler shift caused by the uncertainty in the wind vector corresponding to the wrong pointing of the antennas, and 3rd term is the residual error which includes all the other sources of errors not related to pointing.

Appendix: Pointing errors

- Here we only focus on the pointing related terms (f_{Dpe} and $f_{D\sigma^o}$).
- The overall pointing errors for MetOp second generation are expected to be in the range 0.01°÷0.02°.
- The effect on wind retrieval of 0.01°÷0.02° uncompensated pointing errors is negligible and the corresponding Doppler shift errors (as given by GMFs) are found less than 1 Hz.
- f_{Dpe} is the biggest source of error:

$$\boxed{f_{Derr} = f_D - f_{Dp} \approx f_{Dpe}}$$

- It is possible to correct these errors by measuring the Doppler shifts over land areas, where the shifts are expected to be equal to 0 Hz (residual errors expected to be <1Hz).